Thermal and field-aligned drift effects of the potential created by an altering point charge in a magnetoplasma near the lower oblique resonance

J. Thiel

CENTRE NATIONAL D'ETUDES DES TELECOMMUNICATIONS

CENTRE NATIONAL DE LA RECHERCHE SCIENTIFIQUE

CENTRE DE RECHERCHES EN PHYSIQUE DE L'ENVIRONNEMENT TERRESTRE ET PLANETAIRE

CRPE

NOTE TECHNIQUE
CRPE / 40

Thermal and field-aligned-drift Effects on the potential created by an alternating point charge in a magnetoplasma near the lower oblique resonance

par
J. THIEL

CENTRE NATIONAL D'ETUDES
DES TELECOMMUNICATIONS

CENTRE NATIONAL DE
LA RECHERCHE SCIENTIFIQUE

CENTRE DE RECHERCHE EN PHYSIQUE DE
L'ENVIRONNEMENT TERRESTRE ET PLANETAIRE

NOTE TECHNIQUE CRPE/40

THERMAL AND FIELD-ALIGNED-DRIFT EFFECTS ON THE POTENTIAL CREATED BY AN ALTERNATING POINT CHARGE IN A MAGNETOPLASMA NEAR THE LOWER OBLIQUE RESONANCE

par

J. THIEL

C.R.P.E./P.C.E.

45045 - ORLEANS CEDEX

Le Chef du Département P.C.E.

C. BEGHIN

P. Le Directeur

J. HIEBLOT

Mars 1977

CONTENTS

ABSTRACT

A rapid method is used to find the least-damped root of the dispersion equation for electrostatic waves in a Maxwellian magnetoplasma, including the effects of field-aligned drift ; the low temperature and low-drift-speed approximations are avoided. Calculations are made of the potential created by an alternating point charge at a frequency less than both the plasma and the electron cyclotron frequencies, neglecting collisions, forced ion motion, and the contributions of higher-order roots. A comparison of the numerical results with the approximate expressions previously published shows that the latter are inadequate for diagnostic purposes, i.e. for deducing electron density, temperature, and drift velocity from measurements of the potential.

I. INTRODUCTION

Recent experiments in the laboratory[1-4] and in space[5-7] have confirmed the existence of the so-called cone or oblique resonances of a magnetoplasma in certain frequency bands. If the forced motion of the positive ions is neglected, there are only two such bands : the upper band extends from the upper hybrid frequency down to either the plasma frequency or the electron cyclotron frequency, whichever is the higher ; the lower band extends from the lower of these two frequencies downwards. The present paper is concerned exclusively with the resonance in this lower band, hereinafter referred to as the lower oblique resonance.

In a stationary magnetoplasma, the scalar potential set up by a small monopole antenna has rotational symmetry around the magnetic field line that passes through the antenna and reflexion symmetry with respect to a plane that includes the antenna and is perpendicular to the field lines. Thus, if this antenna is excited with a sinusoidal current of fixed amplitude and frequency, the alternating potential received on a second monopole, at a vector distance $\underset{\sim}{r}$ from the first, depends only on the magnitude r of this distance and on the angle β between $\underset{\sim}{r}$ and the magnetic field direction. Now, in the above frequency bands, if the angle β is varied in the range $0 - \Pi/2$ while r is kept constant, the amplitude of the received potential exhibits quasi-sinusoidal variations ; the alternate maxima and minima correspond to an interference structure. The highest maximum occurs at a certain angle β_o which is that of the so-called resonance cone. The secondary maxima occur only on one side of this cone ; they are regularly speced, and decrease steadily in amplitude as $|\beta - \beta_o|$ increases. Because both the resonance cone angle and the spacing of the secondary maxima depend on the electron density and temperature, it has been suggested that these two parameters could be determined from measurements of the angular variation of the potential.

When the plasma is drifting along the magnetic field, the rotational symmetry of the scalar potential is unaffected but the reflexion symmetry is destroyed : the resonance cone becomes wider upstream and narrower downstream. This angular shift has not yet been detected experimentally, however. Usually it is easier to make precise measurements of frequency rather than of angle, so the suggestion has been made that it would be more fruitful to look for the corresponding shift in resonance frequency at a fixed angle[8]. The sign of the frequency shift depends upon which antenna is transmitting and which is receiving : the shift is towards lower frequencies when the receiver is upstream from the transmitter, and conversely. Measurements of this non-reciprocal effect could be used to determine the electron drift velocity parallel to the magnetic field and hence the field-aligned electron current.

Thermal effects on the angular variations of the potential and of the field created by an alternating point charge in a homogeneous stationary magnetoplasma have already been investigated theoretically, assuming a Maxwellian electron distribution function. Neglecting collisions and forced ion motion, Fisher and Gould[9] and Singh and Gould[10] derived these variation analytically - and calculated their numerically - in the limit of an infinite magnetic field. Later, Kuehl[11,12], Chasseriaux[13] and Burrell[4] extended their calculation to the case in which the magnetic field is finite but they used the low-temperature approximation among others, which drastically simplify the dispersion equation for electrostatic waves : there is only one root, and its damping is neglected. In the present paper, we report numerical calculations of the potential made neglecting collisions and forced ion motion, using the exact dispersion equation, but retaining only the least-damped root, which corresponds to that given by the low-temperature approximation.

The effects of field-aligned drift on the frequency variation of the coupling impedance between two monopoles in a cold homogeneous magnetoplasma have been studied by Storey and Pottelette[14,15]. They neglected collisions and forced ion motion and assumed that the electron plasma frequency was much higher than the cyclotron frequency. Moreover, they considered that the charge supplied to the transmitting monopole antenna by a source of sinusoidally-varying current does not remain on the antenna, but flows straight off it into the plasma, were it joins

in the drift motion. Thus their calculation is not equivalent to that of the potential created by a fixed alternating point charge in the drifting plasma, which is the subject of this paper. In making this calculation, we have again neglected collisions and forced ion motion but we have not made any hypotheses about the characteristic frequencies of the plasma. Moreover, in order to derive an approximate expression for the potential, we have followed an analytical method, used by Kuehl[12] in his investigation of thermal effects, which involves Fourier transforms rather than the Laplace transforms used by Storey and Pottelette.

However, the calculation of the potential including both drift and thermal effects shows that the former may be more important than the latter in some experimental situations in the laboratory and in space[16]. Considering the joint effects of thermal motion and of field-aligned drift, and using the low-temperature approximation, Kuehl[12] has derived an approximate expression for the resonance shift in the limit where the thermal effect is much higher than the drift effect. In this paper, we complete this investigation by studying the opposite limit, where the drift effect is much higher than the thermal effect. Also, we are able to make approximate numerical calculations of the resonance shift for intermediate conditions, since we have included a field-aligned-drift velocity of arbitrary magnitude in our computer programme. This enables us to draw curves of the shift of the resonance frequency versus both electron temperature and drift velocity, without restricting the values of these parameters.

We end this introduction with some remarks about notation and units. Since, in all the cases considered, the potential has cylindrical symmetry around the magnetic field line passing through the monopole, it is convenient to adopt a cylindrical coordinate system and to specify any arbitrary vector function $\underset{\sim}{A}$ of the position vector $\underset{\sim}{r}$ by its component $A_{//}$ (positive or negative) parallel to the field, its perpendicular component $A_{\perp}$ (positive by definition), and the azimuthal angle associated with $A_{\perp}$. Moreover, it happens that in no case is this angle significant, so we shall write simply $\underset{\sim}{r} = (r_{//}, r_{\perp})$ and $\underset{\sim}{A} = (A_{//}, A_{\perp})$. We shall also have occasion to write $\underset{\sim}{A} = A\,\hat{A}$, where $A = |\underset{\sim}{A}|$ and $\hat{A}$ is a unit vector. We use the rationalized MKSA system of units.

II. GENERAL THEORY FOR A DRIFTING MAXWELLIAN MAGNETOPLASMA

An arbitrary alternating (i.e. sinusoidally-varying) source, of angular frequency ω, immersed in a plasma, excites all waves whose wavenumber vectors $\underset{\sim}{k}$ satisfy the dispersion equation $D(\omega, \underset{\sim}{k}) = 0$ and sets up a distribution of scalar potential around itself resulting from the mutual interference of all these waves. The problem of calculating this potential is very difficult if the source perturbs the plasma, so we shall assume that it does not, in which case it can be described completely either as a spatial distribution of alternating charge, or as a distribution of alternating current, the two being related by the condition of charge conservation. If we adopt the convenient gauge condition proposed by Balmain[17], then the scalar potential is the spatial convolution of this distribution with the relevant Green's function, which may be thought of as the potential that would be set up by an alternating unit point charge, even though such an entity is non-physical because it does not satisfy the charge conservation condition[18]. Thus the problem is essentially solved once we have calculated the Green's function, the Fourier transform of which is $(\varepsilon_o \ \underset{\sim}{k} \cdot \underset{\approx}{\varepsilon} \cdot \underset{\sim}{k})^{-1}$, where ε_o is the vacuum permittivity and $\underset{\approx}{\varepsilon}$ is the dielectric tensor of the plasma[19] ; Balmain's gauge condition is equivalent to considering that the alternating point charge excites only electrostatic waves, for which the dispersion equation is $D(\omega, \underset{\sim}{k}) \equiv \underset{\sim}{k} \cdot \underset{\approx}{\varepsilon} \cdot \underset{\sim}{k} = 0$.

Accordingly we wish to calculate the Green's function for a collisionless magnetoplasma drifting along the magnetic field. To begin with, we need the dispersion equation in its explicit form, which depends on the electron distribution function $f(\underset{\sim}{v})$. The latter is assumed to be a shifted Maxwellian

$$f(\underset{\sim}{v}) = (\Pi \ v_{th})^{-3/2} \exp \{- \left[v_{\perp}^{\ 2} + (v_{//} - V_{//})^2 \right] / v_{th}^{\ 2} \} \qquad (1)$$

which is normalized in such a way that $\int f(\underset{\sim}{v}) \ d^3 \underset{\sim}{v} = 1$. The quantity v_{th} is the most probable value of the thermal velocity, and is equal to $(2 \ b \ T_e / m_e)^{1/2}$, where b is Boltzmann's constant, while m_e is the mass of an electron and T_e is the electron temperature of the plasma ;

the drift velocity is $\underset{\sim}{V} = (V_{//}, 0)$. This plasma is also characterized by three other parameters : $\omega_p = (n_e\ e^2/\varepsilon_o\ m_e)^{1/2}$ is the angular plasma frequency (e is the magnitude of the electronic charge and n_e is the electron density of the plasma), $\omega_b = e\ B_o/m_e$ is the angular electron cyclotron frequency ($\underset{\sim}{B}_o$ is the induction vector of the magnetic field), and $r_L = v_{th}/2^{1/2}\ \omega_b$ is the electron Larmor radius (note that the Debye length is not an independent parameter : it is equal to $r_L\ \omega_p/\omega_b$). Another important derived parameter is the upper hybrid resonance frequency $\omega_T = (\omega_p^{\ 2} + \omega_b^{\ 2})^{1/2}$. Throughout this paper, we shall normalize all frequencies with respect to the cyclotron frequency (thus $\Omega_p = \omega_p/\omega_b$, $\Omega_T = \omega_T/\omega_b$ $\Omega = \omega/\omega_b$ and all distances and wavenumber vectors either with respect to the Larmor radius (thus $\underset{\sim}{R} = \underset{\sim}{r}/r_L$ and $\underset{\sim}{K} = \underset{\sim}{k}\ .\ r_L$) or, in section IV, with respect to the characteristic length $\ell = V_{//}/\omega_b$ (thus $\underset{\sim}{\rho} = \underset{\sim}{r}/\ell$ and $\underset{\sim}{\kappa} = \underset{\sim}{k}\ .\ \ell$). With these conventions, the dispersion equation takes the form[19]

$$D(\Omega,\underset{\sim}{K}) \equiv \underset{\sim}{K}.\underset{\approx}{\varepsilon}.\underset{\sim}{K} = K_\perp^{\ 2} + K_{//}^{\ 2} + \Omega_p^{\ 2} \exp(-K_\perp^{\ 2}) \sum_{n=-\infty}^{+\infty} I_n(K_\perp^{\ 2}) \left[1 + \alpha_o F(\alpha_n)\right] = 0 \qquad (2)$$

in which I_n is the modified Bessel function of order n and

$$F(\alpha_n) = i\ \mathrm{sgn}(K_{//})\ \Pi^{1/2}\ \exp(-\alpha_n^{\ 2}) - 2\ \mathrm{erfc}(\alpha_n) \qquad (3)$$

where sgn is the signum function, equal to + 1 or − 1 according to the sign of its argument, and erfc is the complex error, the argument of which is

$$\alpha_n = (\Omega + n - K_{//}\ \ell/r_L)/2^{1/2}\ K_{//} \qquad (4)$$

It is well known that this dispersion equation has an infinite number of roots K for a given direction of the unit vector $\hat{K}$.

At any point in the plasma, the scalar potential is made up of contributions from a double infinity of electrostatic waves (double because all possible $\hat{K}$ - directions are involved). The least-damped-root approximation consists of taking account only of the single infinity of electrostatic waves with the smallest damping for a given $\hat{K}$ - direction. On this basis, the scalar potential - normalized with respect to its vacuum value - created at any point $\underset{\sim}{R}$ by an alternating point charge, located at the origin $\underset{\sim}{R} = 0$, is as given by Kuehl[11] :

$$\psi(\Omega, \underset{\sim}{R}) = i \frac{R}{2} \int_{-\infty}^{+\infty} \exp\,(iK_{//} R_{//}) \frac{H_o^{(1)}(K_{\perp 1} R_{\perp})}{D'(\Omega, K_{//}, K_{\perp 1})} dK_{//} \qquad (5)$$

where $H_o^{(1)}$ is the first Hankel function of zero order and

$$D'(\Omega, K_{//}, K_{\perp 1}) = \left| \partial D(\Omega, K_{//}, K_{\perp}) / \partial (K_{\perp}^2) \right|_{K_{\perp} = K_{\perp 1}} \qquad (6)$$

In Eq. (5) and (6), $K_{\perp 1}$ is the <u>least-damped complex root</u> of the dispersion equation (2), i.e. the one with the smallest imaginary component. Because $K_{//}$ is purely real, $F_o(\alpha_n)$ reduces to the plasma dispersion function $Z(\xi_n)$ of Fried and Conte[20], with $\xi_n = \mathrm{sgn}(K_{//})\, \alpha_n$, which simplifies the dispersion equation (2). Also, because this equation involves no powers of $K_{\perp}$ other than the second, all its roots appear in pairs symmetric about the origin in the complex $K_{\perp}$ plane. Thus, in order to calculate the potential, we must first be able to find this particular root $K_{\perp 1}$, for given Ω_p and Ω, as a function of the variable of integration $K_{//}$.

Before considering how the root $K_{\perp 1}$ can be found in general, we note that analytic expression for it exist in the special case of a cold magnetoplasma. In a stationary cold magnetoplasma, Eq. (2) takes the form

$$D(\Omega, \underset{\sim}{K}) = K_{\perp}^2 + K_{//}^2 + \Omega_p^2 \left[K_{\perp}^2/(1 - \Omega^2) - K_{//}^2/\Omega^2 \right] = 0 \qquad (7)$$

For given Ω_p, Ω, and $K_{//}$, the two possible values for $K_{\perp 1}$ are

$$K_{\perp_1} = \pm \cot g\, \beta_c \cdot K_{//} \tag{8}$$

where

$$\beta_c = tg^{-1} \{ [\Omega^2 (\Omega_T^2 - \Omega^2)] / [(1 - \Omega^2)(\Omega_p^2 - \Omega^2)] \}^{1/2} \tag{9}$$

is the value of β_o in the cold-plasma limit. By introducing collisions which we subsequently neglect[18], we find that the sign of $K_{\perp_1}$ must be negative when $K_{//} > 0$ and positive when $K_{//} < 0$. With this idealized model, the potential becomes infinite on the resonance cone defined by β_c when the frequency is fixed, or at the resonance frequency Ω_c such that

$$\Omega_c^4 - \Omega_c^2 \Omega_T^2 + \Omega_p^2 \sin^2 \beta = 0 \tag{10}$$

when the angle β is fixed. In a cold magnetoplasma with field-aligned drift, the dispersion equation remains simple and still has only one pair of roots which can be found analytically. This case is treated in section IV. These results for a cold magnetoplasma from the background to the rest of this paper, in which we show how they are modified by thermal and field-aligned-drift effects.

In a warm magnetoplasma, the dispersion equation (2) can only be solved numerically[21]. We do so by an iterative method, identifying the least-damped root by continuity with the results for a cold magnetoplasma. Obviously Eq. (2) tends to the cold-magnetoplasma dispersion equation when T_e vanishes, but it also does so for any T_e when the $\underset{\sim}{K}$ vector becomes very small (i.e. $K << 1$). In this limit, the least-damped root of Eq. (2) with a positive imaginary part (which has a negative real part) tends to the purely real negative root of the cold-magnetoplasma dispersion equation. Conversely, if we take this analytic approximation as the initial value, our iterative solution of Eq. (2) always converges to the required root when $|K_{//}| << 1$. Therefore we perform the numerical

integration of Eq. (5) for the potential in such a way that the successive values of $K_{\perp_1}$ ($K_{//}$) are called for in order of increasing $|K_{//}|$ starting from zero. For the first finite value of $K_{//}$, the root $\underline{K}_{\perp_1}$ is found as just described. All subsequent values are found by the same iterative method, but with the initial value obtained by extropolation from the previous values using a polynomial[22]. Thus we follow the path of $\underline{K}_1$ in the complex half-plane Im $K_\perp > 0$ as $|K_{//}|$ increases, even when the latter is no longer small. This procedure is used in sections III and V , our iterative method for finding the complex root of Eq. (2) is an adaptation of the so-called "down-hill" method[23].

Whatever the state of the plasma, the integrand in Eq. (5) for the potential is an oscillating function of $K_{//}$. We evaluate this integral numerically, using Filon's method[24].

III. THERMAL EFFECTS IN A STATIONARY MAXWELLIAN MAGNETOPLASMA

Because recent work, both theoretical and experimental, has been concerned mainly with determining the resonance-cone angle and the interference-structure spacing, we limit our study to the potential distribution created by a point charge alternating at a fixed frequency. Since $V_{//} = 0$, it follows that $D(\Omega, \underset{\sim}{K})$ is an even function of $K_{//}$, so $K_{\perp 1}(K_{//}) = K_{\perp 1}(-K_{//})$ and $D'(\Omega, \underset{\sim}{K}_{//}, K_{\perp}) = D'(\Omega, -K_{//}, K_{\perp})$. Hence the expression for the potential can be written as

$$\psi(\Omega, \underset{\sim}{R}) = iR \int_0^\infty \cos(K_{//} R_{//}) \frac{H_0^{(1)}(K_{\perp 1} R_{\perp})}{D'(\Omega, K_{//}, K_{\perp})} dK_{//} \qquad (11)$$

so $\psi(\Omega, R_{//}, R_{\perp}) = \psi(\Omega, -R_{//}, R_{\perp})$. In view of this symmetry, we need to study the variations of $K_{\perp 1}(K_{//})$ only in the range $K_{//} > 0$ and those of $\psi(\Omega, \underset{\sim}{R})$ only in the range $R_{//} > 0$, i.e. $0 < \beta < \Pi/2$. In this section, we describe the results of numerical calculations of $K_{\perp 1}(K_{//})$ and $\psi(\Omega, \underset{\sim}{R})$ in the particular case where $\Omega_p = 5$.

Our results are presented in order to assess the errors committed by using the formulas given by Kuehl[12] to determine the electron density and temperature of a stationary plasma. These formulas are derived by neglecting the imaginary part of $K_{\perp 1}$, and by taking its real part as equal to the sum of the cold-plasma value [Eq. (8)] and a correction term proportional to $K_{//}^3$. Then the integral of Eq. (11) is calculated analytically with the aid of various other approximations. Hereinafter, this set of approximations will be referred to as the low-temperature analytic (L.T.A.) approximation ; it yields very simple expressions for the angles β_0, β_1, β_2... of the successive maxima of the potential distribution.

THE LEAST-DAMPED ROOT OF THE DISPERSION EQUATION

In Fig. 1 curves are plotted of the real and imaginary parts of $K_{\perp 1}$, as functions of $K_{//}$, for $\Omega_p = 5$ and for various values of Ω. For each of these values, three curves are plotted : the cold-plasma approximation given by Eq. (9), the L.T.A. approximation, and the exact curve derived numerically.

The L.T.A. approximation involves assuming

$$K_{\perp_1}(K_{//}) \simeq -\cot g\, \beta_c\, K_{//} - \alpha K_{//}^3 \qquad (12)$$

where α is the correction coefficient that takes account of the thermal effects[25] :

$$\alpha = 1.5 \frac{\Omega_p^2}{\Omega^3} \left[\frac{1-\Omega^2}{(\Omega_T^2-\Omega^2)(\Omega_p^2-\Omega^2)}\right]^{1/2} \left[1 - \frac{\Omega^2(2\Omega^4-\Omega^2+1/3)}{(1-\Omega^2)^3}\cot g^2\beta_c + \frac{\Omega^4}{(1-\Omega^2)(4-\Omega^2)}\cot g^4\beta_c\right] \qquad (13)$$

It is important to note that α vanishes for a particular value Ω_α of Ω which depends only on Ω_p ; for $\Omega_p = 5$, we have $\Omega_\alpha \simeq 0{,}692$. When $\Omega < \Omega_\alpha$ (e.g. $\Omega = 0.1$ and $\Omega = 0.5$), the coefficient α is positive and the L.T.A. curves lie below the cold-plasma straight line, which is inclined at the angle β_c to the negative Re $K_{\perp_1}$ - axis. When $\Omega = \Omega_\alpha$, the coefficient α vanishes and there is no interference structure : the L.T.A. approximation fails to predict any thermal effects. When $\Omega > \Omega_\alpha$ (e.g. $\Omega = 0.9$), α is negative and the L.T.A. curve lies above the cold-plasma curve. Thus the nature of the L.T.A. approximation depends on whether the normalized frequency is greater or less than Ω_α ; the physical significance of this value has not yet been identified.

The results of our numerical calculations are plotted as curves of Re $K_{\perp_1}$ and of Im $K_{\perp_1}$ versus $K_{//}$, for positive real values of this variable. Thus they refer to inhomogeneous waves with Im $K_{//} = 0$, rather than to the homogeneous waves (i.e. waves in which the vectors Re $(\underset{\sim}{K})$ and Im $(\underset{\sim}{K})$ are parallel to one another) that have been studied by some previous authors[26]. Our results are similar to the L.T.A. approximation for fast electrostatic waves ($\underset{\sim}{K} \sim 0$) in a range of $K_{//}$ which depends on Ω. When $\Omega < \Omega_\alpha$, the curve of Re $\underset{\sim}{K}_1$ is well approximated by Eq. (12), while the curve of Im $K_{\perp_1}$ is very close to the $K_{//}$ - axis up to a certain value of $K_{//}$ which increases with increasing frequency. Above this value, the curves derived from Eq. (12) do not bend in the right direction. When $\Omega = \Omega_\alpha$, the exact curve of Re $K_{\perp_1}$ lies below the cold-plasma straight line over a large range of $K_{//}$. When Ω is greater than Ω_α, the curve for

Re $K_{\perp_1}$ from Eq. (12) bends in one direction only, whereas the exact curve is more complex and lies above the cold-plasma line for small $K_{//}$ and below it for large $K_{//}$; thus the discrepancies between these two curves are now very significant. Moreover, the value of $K_{//}$ above which Im $K_{\perp_1}$ can no longer be ignored now decreases with increasing frequency. In short, the L.T.A. approximation does not give a good account of the behaviour of the least-damped waves when the frequency is near the gyrofrequency ; however, precise information about its range of validity can be obtained only by numerical calculation of the potential.

THE POTENTIAL CREATED BY AN ALTERNATING POINT CHARGE

The preceding three sets of curves for the least-damped root of the dispersion relation lead to very different potential distributions near the lower oblique resonance.

Let us recall that, in the cold-plasma approximation, the potential is[18]

$$\psi(\Omega,\beta) = \left[1 + \Omega_p{}^2/(1 - \Omega^2)\right]^{-1/2}\left[-1 + \Omega_p{}^2/\Omega^2\right]^{-1/2} (\cos\beta)^{-1}\left[\mathrm{tg}^2\beta - \mathrm{tg}^2\beta_c\right]^{-1/2} \qquad (14)$$

It is infinite on the resonance cone, which has a semi-apical angle β_c, and it decreases smoothly with increasing $|\beta - \beta_c|$ on both sides of this cone.

In contrast, the L.T.A. approximation for the potential is

$$\underset{\sim}{\psi}(\Omega,R) = \frac{(-i)^{2/3}}{3(2\Pi)^{1/2}} \frac{\tan^{1/2}\beta_c}{\sin^{2/3}\beta_c} \frac{1}{1+\Omega_p{}^2/(1-\Omega^2)} \frac{R^{1/3}}{|\alpha|^{1/6}} F(z_T) \qquad (15)$$

where $F(z_T)$ is a function defined and graphed in Ref. 10 ; its argument, which is purely real, is

$$z_T = \left[R^{2/3}/(|\alpha|^{1/3} \sin^{4/3}\beta_c)\right] (\beta_c - \beta) \qquad (16)$$

The predictions of the L.T.A. approximation differ from those of the cold-plasma approximation in three main respects. Firstly, the potential remains finite on the resonance cone. Secondly, this maximum of potential occurs at a slightly different angle :

$$\beta_o \sim \beta_c - 1.8 \text{ sgn } (\Omega_\alpha - \Omega) \ |\alpha|^{1/3} \sin^{4/3} \beta_c \ R^{-2/3} \tag{17}$$

The amount of the change in the angle β at resonance depends both on the frequency and on the electron temperature(it is proportional to $T_e^{1/3}$), but its sign depends on the frequency alone : the L.T.A. resonance cone lies inside the cold-plasma resonance cone if $\Omega < \Omega_\alpha$, and outside it if $\Omega > \Omega_\alpha$. Thirdly, there appears a quasi-periodic interference structure, in which the minima are zeros and the maxima decrease in amplitude with increasing angular distance from the resonance cone. The angular positions of these secondary maxima are approximately

$$\beta_n \approx \beta_c - 3 \left[(n+0.25)\Pi\right]^{2/3} \text{sgn } (\Omega_\alpha - \Omega) \left|\alpha\right|^{1/3} \sin^{4/3} \beta_c \ R^{-2/3} \tag{18}$$

where n = 1, 2, 3,... Again, their angular spacing depends on Ω and is proportional to $T_e^{1/3}$. The entire structure occurs inside the L.T.A. resonance cone when $\Omega < \Omega_\alpha$ and outside it when $\Omega > \Omega_\alpha$. In the rest of this section we shall compare these predictions of the L.T.A. approximation with the results of our more precise numerical calculations, in order to establish whether or not the L.T.A. formulas are adequate for diagnostic purposes.

When the electron temperature is such that $R \gg 1$, the L.T.A. approximation leads to a potential distribution in reasonably good agreement with the more precise calculations so long as the excitation frequency is not too close to the electron gyrofrequency, or more exactly, so long as $\Omega \ll \Omega_\alpha$. This fact is illustrated in Fig. 2, where the variations of $|\psi|$ given by our computer programme (solid curve) and by Eq. (15) (dashed curve) are plotted for the case where $\Omega_p = 5$, R = 100 and $\Omega = 0.5$. It appears

that the damping of the maxima at β_0 and β_1 is underestimated by the L.T.A. approximation ; moreover, the prediction that the minima should be true zeros is not confirmed by the numerical calculations. We have verified in numerous instances that these slight discrepancies presist for other values of Ω_p, of R and of Ω ; probably they are due to the fact that the damping of the electrostatic waves is neglected in the L.T.A. approximation.

Let us now consider how the potential distribution in the plasma changes as the normalized excitation frequency Ω varies from 0 to 1. In Fig. 3, we have plotted the angles β_0, β_1 and β_2 of the successive maxima of the potential distribution as given by our programme (solid curves) and by Eq. (17) and (18) (dashed curves) for the case where R = 100. The true resonance cone (i.e. the maximum at β_0) always lies inside that given by the cold-plasma approximation, contrary to the result given by the approximate L.T.A. formula of Eq. (17). As regards the secondary maxima at β_1 and β_2, the corresponding formula of Eq. (18) again disagrees with our more precise calculation which show that this interference structure always lies inside the resonance cone. Moreover, as the frequency approaches the gyrofrequency, the amplitude of each of these secondary maxima diminishes progressively, in comparison with that of the main maximum on the resonance cone : the higher the order of the secondary maximum, the more rapid is the decrease. In the particular case of Fig. 3, no secondary maxima are discernible when Ω is greater than about 0.8. Thus exact numerical calculations of the potential show that the validity of the L.T.A. approximation depends not only on the temperature but also on the frequency.

When the excitation frequency is fixed in relation to the gyrofrequency, the potential distribution due to a point charge is strongly affected by variations of the electron density or temperature of the plasma. For brevity, we now limit our study to the influence of the temperature, and to the particular case where Ω = 0.5 and Ω_p = 5. Fig. 4 shows how the angles β_0, β_1 and β_2 vary when the Larmor radius is increased from 0.001 r (R = 1 000) to 0.1 r (R = 10) ; the results of the numerical integration for the potential have been plotted as the solid curves, while Eq. (17) and (18) yield the dashed curves. These two sets of curves agree

qualitatively. However, Eq. (17) yields too small a value for β_0, while Eq. (18) gives too large a value for β_1 especially when k is small. These two errors add constructively in the calculation of the interference-structure spacing $\beta_0 - \beta_1$, so when measurements of this spacing are interpreted using the L.T.A. approximation, the estimated temperature is too high.

Now if the electron temperature is to be determined accurately, the potential measurements must be made at a distance from the source at which the interference spacing is very sensitive to variations of this temperature. For instance, if $\Omega_p = 5$ and $\Omega = 0.5$ (Fig. 4) this condition is fulfilled if $R \sim 100$, in which case $\beta_0 - \beta_1$ varies rapidly as a function of R ; a measured interference spacing of 20° would then be interpreted as corresponding to R = 60 on the basis of our numerical results, but as R = 48 by the L.T.A. method based on Eq. (17) and (18). The latter yields a temperature which is about 56 % higher than the true value. This result is typical, and we conclude that the L.T.A. formulas are inadequate for determining electron temperatures[26].

Under most experimental conditions, the electron density is not known in advance, but it can be deduced, together with the temperature, from joint measurements of the interference spacing and of the resonance cone angle. We find that the errors in density introduced by using Eq. (17) and (18) are greatest for values of Ω_p near 1, where the potential distribution is strongly affected by density variations. For instance, some potential measurements in the auroral ionosphere by Gonfalone[28] yield $T_e = 655°$ K and $n_e = 7.8 \times 10^4$ cm^{-3} ($\Omega_p = 1.82$) when interpreted by means of the formulas of Eq. (17) and (18), but $T_e = 569°$ K and $n_e = 13.1 \times 10^4$ cm^{-3} ($\Omega_p = 2.36$) when our computer programme is used. To facilitate extensive interpretation of the angular variations of the potential we have drawn up a set of charts on which lines corresponding to constant values of the angles β_0, β_1, β_2, ... are plotted in the (T_e, n_e) plane[7] ; pairs of values of electron temperature and density, together with error bars, can be read off easily from these charts.

IV. DRIFT EFFECTS IN A COLD MAGNETOPLASMA

In a moving magnetoplasma, the dispersion equation for electrostatic waves is modified by the Doppler effect, so the interference structure in the potential distribution due to an alternating point charge is sensitive to the motion. To study this effect near the lower oblique resonance, we assume that the plasma is drifting in the direction of the applied static magnetic field ($V_{//} > 0$) and we neglect the dissipative processes, namely thermal motion and collisions. The dispersion equation of the electrostatic waves is then derived from that for a stationary magnetoplasma, as given by Eq. (7), by replacing ω by $\omega - k_{//} V_{//}$ (i.e. Ω by $\Omega - \kappa_{//}$). Thus

$$D(\Omega,\underset{\sim}{\kappa}) = \kappa_{\perp}^2 + \kappa_{//}^2 + \Omega_p^2 \left[\frac{\kappa_{\perp}^2}{1-(\Omega-\kappa_{//})^2} - \frac{\kappa_{//}^2}{(\Omega-\kappa_{//})^2} \right] \tag{18}$$

and the expression for the potential becomes

$$\psi(\Omega,\underset{\sim}{\rho}) = i \frac{\rho}{2} \int_{-\infty}^{+\infty} \frac{1-(\Omega-\kappa_{//})^2}{\Omega_T^2-(\Omega-\kappa_{//})^2} H_o^{(1)} (\rho_{\perp}\kappa_{\perp_1}) \exp (i\rho_{//}\kappa_{//}) \, d\kappa_{//} \tag{19}$$

where $\kappa_{\perp_1}$ is the root of Eq. (18) with a positive imaginary part (the choice of root when both are purely real is explained below). In this section, we first discuss how $\kappa_{\perp_1}$ varies when $\kappa_{//}$, the real variable of integration, varies from $-\infty$ to $+\infty$; then we present both exact numerical and approximate analytic calculations of the potential given by Eq. (19).

THE ROOT OF THE DISPERSION EQUATION

From Eq. (18), the roots of the dispersion equation[29] $D(\Omega, \underset{\sim}{\kappa}) = 0$ are given by

$$\kappa_{\perp_1}^2 = \kappa_{//}^2 \left[\frac{(\Omega-\kappa_{//})^2-\Omega_p^2}{(\Omega-\kappa_{//})^2-\Omega_T^2} \right] \left[\frac{1}{(\Omega-\kappa_{//})^2} - 1 \right] \tag{20}$$

which shows that they vanish for $\kappa_{//} = 0$ or $\Omega \pm 1$ or $\Omega \pm \Omega_p$ and go to $\pm \infty$ for $\kappa_{//} = \Omega$ or $\Omega \pm \Omega_T$. These eight particular values - marked by dots on the vertical axis in Fig. 5.a - delimit nine branches of the curve $\kappa_{\perp_1}(\kappa_{//})$, on each of which $\kappa_{\perp_1}$ has two possible values, of opposite sign, which are either purely imaginary (when $\kappa_{\perp_1}^2$ is negative) or purely real (when $\kappa_{\perp_1}^2$ is positive). In the first case, we take only the root with a positive imaginary part ; there are four such branches (the dotted lines in Fig. 5.a.), on all of which the waves are strongly damped and make no appreciable contribution to the potential. In the second case, the sign of $\kappa_{\perp_1}$ is chosen by introducing an infinitesimal amount of collisions, and we find that it is positive when $\Omega < \kappa_{//} < \Omega + 1$ or $\Omega - \Omega_T < \kappa_{//} < \Omega - \Omega_p$, but negative when $\Omega + \Omega_p < \kappa_{//} < \Omega + \Omega_T$ or $\Omega - 1 < \kappa_{//} < 0$ or $0 < \kappa_{//} < \Omega$ (the solid lines in Fig. 5.a.). To these five branches correspond five sets of undamped waves, all of which have to be considered in a quantitative analysis. However, the numerical calculation of the potential in the next subsection will show that the drift effect can be analyzed qualitatively by considering only the two branches that start at the origin $\underset{\sim}{\kappa} = 0$.

These two, which are shown in greater detail in Fig. 5.b. (solid lines), are deformed versions of the two sole branches that exist when the plasma is stationary (broken lines). They are tangent to the latter at the origin, so they may be expected to make the principal contribution to the potential at and near the lower oblique resonance. Because the curves $\kappa_{\perp_1}(\kappa_{//})$ for a drifting plasma lie below the corresponding straight line for a stationary plasma, it follows that the resonance cone becomes narrower downstream and wider upstream when the plasma drifts. (For the relationship between the dispersion curves and the resonance-cone angle, see Ref. 26). An approximate expression for the parts of these curves nearest to the origin may be obtained by expanding the right-hand side of Eq. (20) as a power series, and taking just the first two terms[12] :

$$\kappa_{\perp_1} \approx - \operatorname{cotg} \beta_c \, |\kappa_{//}| - \gamma \, |\kappa_{//}| \, \kappa_{//} \qquad (21)$$

where

$$\gamma = \Omega_p^{\,2}\,\Omega^2\,(1-\Omega^2)^{-1/2}\,(\Omega_T^{\,2}-\Omega^2)^{-3/2}\,(\Omega_p^{\,2}-\Omega^2)^{-1/2}\,(\Omega_T^{\,2}-2\Omega^2) \qquad (22)$$

The corresponding curve is plotted as a dashed line in Fig. 5.b. for the case where $\Omega_p = 5$ and $\Omega = 0.5$. There are discrepancies from the exact curve when $|\kappa_{//}|$ is so large that the second-order term in Eq. (21) is no longer small compared with the first-order term. Roughly speaking, the approximation is reasonable when

$$|\kappa_{//}| \ll \text{cotg}\ \beta_c/\gamma \qquad (23)$$

($\gamma = 4.55$ in the case of Fig. 5.b. so this inequality is $|\kappa_{//}| \ll 0.37$). Subject to this condition, Eq. (21) should be useful as the basis for an approximate analytic study of how the frequency variation of the potential at a fixed point is modified when the plasma drifts. But before doing this, we present the results from a precise numerical study of the same question, in the course of which we confirm that the main resonance and other regular features of the frequency variation are indeed attributable to the two branches of the dispersion curve $\kappa_{\perp 1}(\kappa_{//})$ that start at the origin.

NUMERICAL CALCULATION OF THE POTENTIAL

Since it has been suggested that the field-aligned drift velocity could be deduced from the shift in frequency that occurs when the emitting and receiving electrodes are interchanged, we consider mainly the frequency variation of the potential at two fixed points, at equal distances from the source but in opposite directions. The calculation involves integrating an oscillating function, which we do numerically by Filon's method[24]. The results are plotted as the thin curves of Fig. 6.a. and 6.b. for the case where $\Omega_p = 5$ and $\rho = 160$. The curve ψ_- in Fig. 6,a. shows the potential calculated for $\beta = 150°$ while the curve ψ_+ in Fig.6.b. is for $\beta = 30°$; the subscript is the sign of the component of drift velocity along the line from the source (transmitter) to the point of observation (receiver), so in the first case the receiver is upstream from the transmitter, and in the second it is downstream. When the plasma is stationary, the curve is the same in both directions and the resonance

frequency is $\Omega_c = 0.493$. When the plasma is in motion and the receiver is upstream, the resonance frequency Ω_{-_0} is shifted towards the lower frequencies ($\Omega_c - \Omega_{-_0} \sim 0.11$), and a regular interference structure appears at frequencies below the main resonance frequency ; here we call the successive secondary resonance frequencies Ω_{-_1}, Ω_{-_2}, etc... When the receiver is downstream from the transmitter, these results are inverted : the resonance frequency Ω_{+_0} is greater than Ω_c ($\Omega_{+_0} - \Omega_c \sim 0.13$) and an interference structure, in this case with only one peak, appears above Ω_{+_0} at a frequency called Ω_{+_1}. Moreover, there are irregular oscillations in the low-frequency range of the curve of ψ_+. These results are similar to those of Storey and Pottelette but our use of the Fourier transform rather than the Laplace transform enables us to identify the branches of the dispersion curve that are responsible for the irregular oscillations of the potential downstream from the transmitter[30].

The contribution made by each of the nine branches of the dispersion curve to the potential can be analyzed quantitatively by restricting of Eq. (19) to the corresponding range of the variable $\kappa_{//}$. To begin with, we consider the contributions from the two branches that start at the origin $\kappa_{//} = 0$, so we perform a partial integration from $\Omega-1$ to 0 for ψ_- and from 0 to Ω for ψ_+. The thick curve in Fig. 6.a. shows the result of such an incomplete calculation of the potential ψ_- upstream from the transmitter, obtained by considering only the contribution from the branch $\Omega-1 < \kappa_{//} < 0$. Comparison with the exact curve of $|\psi_-|$ shows that the frequencies Ω_{-_0}, Ω_{-_1}, Ω_{-_2} of the successive maxima are only slightly modified in spite of the discrepancies in their magnitudes. Similarly, the result of the partial integration from 0 to Ω for the potential ψ_+ downstream from the transmitter is sketched as the thick line in Fig. 6.b. Here again, the characteristic frequencies of the main resonance and of the regular interference structure are practically unaffected. Moreover the irregular oscillations are suppressed, so we conclude that they are due to undamped electrostatic waves with wave vector components $\kappa_{//}$ outside the range from 0 to Ω, interfering with the waves for which the $\kappa_{//}$ lie in this range. These results are consistent with the notion that the waves with relatively large κ only contribute to the potential downstream from the transmitter, because their group velocity vectors $\underset{\sim}{V}_g$ are such that $\underset{\sim}{V}_g \cdot \underset{\sim}{V} > 0$. Thus, in order to study the shift in resonance frequency and the interference-structure spacing, it is sufficient to confine our attention to the branches $\Omega-1 < \kappa_{//} < 0$ and $0 < \kappa_{//} < \Omega$ for ψ_+.

ANALYTIC APPROXIMATION FOR THE POTENTIAL

In the light of the preceding subsection, we limit the integration for the potential to a single branch of the curve $\kappa_{\perp_1}(\kappa_{//})$, but some further approximations must be made before we can perform this integration analytically :

(i). The first approximation is to use the Eq. (21) for $\kappa_{\perp_1}$. Assuming that

$$\rho >> \Omega_p^{\,3}\Omega_c^{\,-1}(1-\Omega_c^{\,2})^{-3/2}(\Omega_T^{\,2}-\Omega_c^{\,2})^{-3/2}(\Omega_p^{\,2}-\Omega_c^{\,2})^{-3/2}(\Omega_T^{\,2}-2\Omega_c^{\,2}) \qquad (24)$$

we have $|\rho_\perp \kappa_{\perp_1}| >> 1$ at both limits of the range of $\kappa_{//}$ where the approximation (21) is valid ; these limits are defined by the inequality (23). By using the saddle-point method together with the asymptotic expansion of the Hankel function, we find that the corresponding frequency range of validity for Eq. (21) is

$$|\Omega - \Omega_c| << 2\Omega_c\,(1 - \Omega_c^{\,2}) \qquad (25)$$

(ii). The second approximation is to extend the outer limit of integration for the potential from $\Omega-1$ to $-\infty$ for ψ_-, and from Ω to $+\infty$ for ψ_+. This is correct if the range of $\kappa_{//}$ where the Eq. (21) is valid is entirely included in the interval between $\Omega-1$ and Ω, which implies that the frequency is such that

$$\frac{(1 - \Omega^2)(\Omega_p^{\,2} - \Omega^2)(\Omega_T^{\,2} - \Omega^2)}{\Omega_p^{\,2}(\Omega_T^{\,2} - 2\Omega^2)} < \min\left(1, \frac{1 - \Omega}{\Omega}\right) \qquad (26)$$

On this condition, we may neglect $\kappa_{//}$ in the non-oscillatory term in the integrand of Eq. (19) ; the latter may then be rewritten

$$\psi_{\pm}(\Omega,\underset{\sim}{\rho}) \underset{\sim}{\simeq} i\,\frac{\rho}{2}\,\frac{1-\Omega^2}{\Omega_T{}^2\,\Omega^2}\int_0^{\infty} H_o^{(1)}\left[\rho_{\perp}(-\cot g\beta_c|\kappa_{//}|+\gamma|\kappa_{//}|\kappa_{//})\right]\exp(i\rho_{//}\kappa_{//})d\kappa_{//} \tag{27}$$

Using a method due to Kuehl[12], we evaluate this integral by splitting it into two parts, as follows :

$$\psi_{\pm}(\Omega,\underset{\sim}{\rho}) = i\,\frac{\rho}{2}\,\frac{1-\Omega^2}{\Omega_T{}^2-\Omega^2}\left(I_1 + I_{\pm}\right) \tag{28}$$

where

$$I_1 = \frac{1}{2}\int_{-\infty}^{+\infty}\left\{H_o^{(1)}\left[\rho_{\perp}(-\cot g\beta_c|\kappa_{//}|+\gamma|\kappa_{//}|\kappa_{//})\right] - \frac{\Pi}{2i}\,\rho\,\cot g\beta_c|\kappa_{//}|^{1/2}\right.$$
$$\left. x\,\exp\left[i\rho_{\perp}(-\cot g\beta_c|\kappa_{//}|-\gamma|\kappa_{//}|\kappa_{//}\right]\right\}\exp(i\rho_{//}\kappa_{//})\,d\kappa_{//} \tag{29}$$

$$I_+ = \left(\frac{\Pi}{2i}\,\rho_{\perp}\cot g\beta_c\right)^{1/2}\int_0^{\infty}\exp\left[i(\rho_{//}-\rho_{\perp}\cot g\beta_c)\kappa_{//} - i\rho_{\perp}\gamma\kappa_{//}{}^2\right]\kappa_{//}{}^{-1/2}\,d\kappa_{//} \tag{30}$$

$$I_- = \left(\frac{\Pi}{2i}\,\rho_{\perp}\cot g\beta_c\right)^{1/2}\int_{-\infty}^{0}\exp\left[i(\rho_{//}+\rho_{\perp}\cot g\beta_c)\kappa_{//} + i\rho_{\perp}\gamma\,\kappa_{//}{}^2\right](-\kappa_{//})^{-1/2}\,d\kappa_{//} \tag{31}$$

(iii) The third approximation is to neglect the contribution of I_1. This final approximation is valid if

$$\rho >> (\Omega_T{}^2-\Omega_c{}^2)(\Omega_p{}^2-\Omega_c{}^2)^{-1}(1-\Omega_c{}^2)^{1/2} \tag{32}$$

From here on, we shall refer to these three assumptions collectively as the low-drift analytic (L.D.A.) approximation.

In this approximation, the potential created by an alternating point charge is

$$\psi_{\pm}(\Omega,\underset{\sim}{\rho}) \approx i\,\frac{\rho}{2}\,\frac{1-\Omega^2}{\Omega_T^{\,2}\;\Omega^2}\left[\frac{2\,i}{\Pi\rho_{\perp}\,\mathrm{cotg}\beta_c}\right]^{1/2}\int_0^{\infty}\exp\left\{\pm i\left[(\rho_{//}\pm\rho_{\perp}\mathrm{cotg}\beta_c)\kappa_{//}-\rho_{\perp}\gamma\kappa_{//}^{\,2}\right]\right\}\kappa_{//}^{\,-1/2}d\kappa_{//} \tag{33}$$

The new integral on the right hand side depends only on the parameter $\zeta_{\pm} = \rho_{\perp}^{-1/2}\gamma^{-1/2}(\rho_{//}\pm\rho_{\perp}\mathrm{cotg}\beta_c)$ and can be rewritten

$$\int_0^{\infty}\exp\left\{\pm i\left[(\rho_{//}\pm\rho_{\perp}\mathrm{cotg}\beta_c)\kappa_{//}-\rho_{\perp}\gamma\kappa_{//}^{\,2}\right]\right\}\kappa_{//}^{\,-1/2}d\kappa_{//} = \frac{1}{2}\,(i\rho_{\perp}\gamma)^{-1/4}\Phi_{\pm}(\zeta_{\pm}) \tag{34}$$

where $\Phi_+(\zeta_+)$ is an integral which may be evaluated by using a new variable of integration $t = i\rho_{\perp}\gamma\kappa_{//}^{\,2}$ and by changing the upper limit of integration from $i\infty$ to $+\infty$[31] :

$$\Phi_+(\zeta_+) = \int_0^{\infty}\exp\,(i^{1/2}\zeta_+ t^{1/2}-t)\;t^{-3/4}dt \tag{35}$$

By developing the exponential as a power series and using the integral definition of the gamma function (Γ)[32], one obtains the following series expansion :

$$\Phi_+(\zeta_+) = \sum_{n=o}^{\infty}\exp(in\Pi/4)\;\Gamma(\frac{n}{2}+\frac{1}{4})\zeta_+^{\,n}/n! \tag{36}$$

The asymptotic forms of Eq. (35) may be derived by the method of steepest descents ; they are

$$\Phi_+(\zeta_+) \approx 2i^{3/4}(\Pi/\zeta_+)^{1/2}\left[1-i\sqrt{2}\exp(i\zeta_+^{\,2}/4)\right] \qquad \text{if } \zeta_+ >> 0 \tag{37.a.}$$

$$\Phi_+(\zeta_+) \approx 2(-i)^{1/4}(-\Pi/\zeta_+)^{1/2} \qquad \text{if } \zeta_+ << 0 \tag{37.b.}$$

The procedure for evaluating $\Phi_-(\zeta_-)$ is similar, except that ζ_+ is replaced by ζ_- and i is replaced by - i ; thus $\Phi_-(\zeta_-)$ is the complex conjugate of $\Phi_+(\zeta_-)$. The modulus of $\Phi_+(\zeta_+)$ is graphed versus ζ_+ in Fig. 7. By inserting this function into Eq. (33), we obtain

$$\psi_\pm(\Omega,\rho) \underset{\sim}{\approx} - (8\Pi\cot g\beta_c)^{-1/2}\rho_\perp^{-3/4}\gamma^{-1/4}\Phi_\pm(\zeta_\pm) \tag{38}$$

This is the L.D.A. approximation for the potential.

Let us now use this result to derive approximate formulas for the resonance-frequency shift and the interference -structure spacing. At a fixed angle β, with the frequency varying, it is more convenient to use the expression

$$\zeta_\pm \underset{\sim}{\approx} \pm\rho^{1/2}\Omega_c^{-1/2}\Omega_p^{-3/2}(\Omega_T^2-\Omega_c^2)^{1/2}(\Omega_T^2-2\Omega_c^2)^{1/2}(1-\Omega_c^2)^{-1/4}(\Omega_p^2-\Omega_c^2)^{3/4}(\Omega-\Omega_c) \tag{39}$$

which applies when $\Omega \underset{\sim}{\approx} \Omega_c$. Since this approximation is linear, the shift of the resonance frequency, for a given drift velocity has the same magnitude (but opposite sign) downstream and upstream from the transmitter. The function $|\Phi_+(\zeta_+)|$ is maximum for $\zeta_+ = 2.199$, so the <u>differential shift</u> (i.e. the difference between the downstream and upstream resonance frequencies, which is what one would measure experimentally) is

$$\Delta\Omega = \Omega_{+_0}-\Omega_{-_0} \underset{\sim}{\approx} 4.398\rho^{-1/2}\Omega_c^{1/2}\,\Omega_p^{3/2}(\Omega_T^2-\Omega_c^2)^{-1/2}(\Omega_T^2-2\Omega_c^2)^{-1/2}(1-\Omega_c^2)^{1/4}(\Omega_p^2-\Omega_c^2)^{-3/4} \tag{40}$$

In the limiting case where the plasma density is infinite ($\Omega_p \to \infty$), we have $\Omega_T \underset{\sim}{\approx} \Omega_p$ and $\Omega_c \underset{\sim}{\approx} \sin\beta$; hence Eq. (40) becomes

$$\Delta\Omega \underset{\sim}{\approx} 4.398\rho^{-1/2}\sin^{1/2}\beta\,\cos^{1/2}\beta \underset{\sim}{\approx} 1.755\left(\Pi V_{//}\sin 2\beta/r\omega_b\right)^{1/2} \tag{41}$$

A similar result has been derived previously by Pottelette[33], and we have expressed ours in the same form ; however, he gives the numerical factor before the bracket as 2. An analytic formula also can be derived for the first frequency interference spacing when the angle is fixed, using the fact that the first secondary maximum of $|\Phi_+(\zeta_+)|$ occurs for $\zeta_+ = 5.4$; in the limiting case where $\Omega_p \to \infty$, we find

$$\Omega_{+_1} - \Omega_{+_0} \approx \Omega_{-_0} - \Omega_{-_1} \approx 1.27 \left(\Pi V_{//} \sin 2\beta / r\omega_b\right)^{1/2} \tag{42}$$

In the analogous formula derived by Pottelette[33], the numerical factor is 1.0. Similar approximations can be derived readily for the resonance angle shift and interference-structure spacing at fixed frequency.

To summarize, our analysis based on the L.D.A. approximation leads to results of the same functional form as those previously published, but of slightly different magnitude. In particular, we confirm that the shift in the resonance and the interference spacing due to the drift along the magnetic field are proportional, in a cold magnetoplasma, to the square root of the drift velocity. It is important to reconcile this result with the linear proportionality discovered by Kuehl[12] in the case of warm drifting magnetoplasma.

V. COMBINED EFFECTS OF THERMAL AND DRIFT MOTIONS

In this section, we consider how the potential distribution created in a warm magnetoplasma is modified by the joint action of the thermal and drift motions, which have been treated separately in the two preceding sections. Downstream from the transmitter, the effects of both these motions are to close up the resonance cone and to create a regular interference structure within it. Upstream from the transmitter, the thermal motion has the same effect, but the drift motion opens up the resonance cone and gives rise to a regular interference structure outside it. In studying the resultant potential distribution, both analytically and numerically, we again neglect ions and collisions and adopt the least-damped-root approximation. Analytically, Kuehl[12] has already derived some approximate formulas on the further asumption that $r_\perp << \alpha^2 \, r_L^{\,4}/\gamma^3 \, \ell^3$; we find that his method of calculation is also applicable to the case where $r_\perp >> \alpha^2 \, r_L^{\,4}/\gamma^3 \, \ell^3$. Numerically, of course, it is possible to calculate the potential distribution for arbitrary values of the thermal and drift velocities[34]. In this section, we first analyze the behaviour of the least-damped root of the dispersion equation for electrostatic waves in a drifting Maxwellian magnetoplasma, then we complete the analytic calculations of Kuehl for the case where $r_\perp >> \alpha^2 \, r_L^{\,4}/\gamma^3 \, \ell^3$, and finally we present the results of some numerical calculations of the potential.

THE LEAST-DAMPED ROOT OF THE DISPERSION EQUATION

In Fig. 8, the exact values of Re $K_{\perp_1}$ (thick solid line) and of Im $K_{\perp_1}$ (thick dashed line) are plotted as functions of $K_{//}$, for $\Omega_p = 5.$, $\Omega = 0.5$ and $\ell/r_L = 0.25$. The corresponding purely real values of $K_{\perp_1}$ for a stationary cold plasma are also graphed, as the thin broken line, while the thin solid line represents a purely real approximation to $K_{\perp_1}$, including thermal and drift effects, which we shall use in our analytic calculation of the potential.

This approximation for $K_{\perp_1}$ is obtained by expanding the complete dispersion equation - Eq. (2) - as a power series in terms of the variables $K_\perp$ and $K_{//}$. Near the origin $\underset{\sim}{K} \sim 0$, it is sufficient to retain only the three leading termes, so

$$K_{\perp_1}(K_{//}) \approx - \operatorname{cotg} \beta_c \, |K_{//}| - \gamma \frac{\ell}{r_L} |K_{//}| K_{//} - \alpha \, |K_{//}| K_{//}^2 \qquad (43)$$

where α and γ are defined by Eq. (13) and (22) respectively. In this approximation, the thermal and drift effects are not coupled, inasmuch as the expression for $K_{\perp_1}$ is the sum of the thermal correction term from Eq. (12) - illustrated in Fig. 1 - and the drift correction term from Eq. (21) - illustrated in Fig. 5.b. - added to the expression of Eq. (8) for the case of a cold stationary plasma. For positive values of $K_{//}$, the curve representing this approximation to the least-damped root always lies below the cold-plasma straight line (as in Fig. 8) if $\alpha > 0$, i.e. if $\Omega < \Omega_\alpha$. When $\Omega_\alpha < \Omega < 1$, this curve lies below the straight line if $K_{//} < \gamma r_L/\alpha\ell$ and above it if $K_{//} > \gamma r_L/\alpha\ell$. For negative values of $K_{//}$, the situation is as follows : when $\Omega < \Omega_\alpha$, the approximate curve leaves the origin below the cold-plasma straight line, then crosses this line at the point where $K_{//} = - \gamma r_L/\alpha\ell$ and thereafter lies above it ; when $\Omega_\alpha < \Omega < 1$, the curve always lies below the line. Thus the behaviour of the least-damped root, as given by this <u>low temperature and drift</u> (L.T.D.) approximation, depends not only on the relative values of the thermal and drift velocities but also on the frequency.

The exact values of $K_{\perp_1}$, calculated by using the iterative <u>complex-root-finding</u> method described at the end of section II, are similar to the preceding approximate values only for fast electrostatic waves with $K \lesssim 0$. For large values of $|K_{//}|$, the discrepancies that have been described separately in sections III and IV now occur jointly. Depending on the frequency Ω and on the sign of $K_{//}$, the disagreements due to the thermal and drift effects either add to or substract from one another, and so reduce or enlarge the range of $K_{//}$, around the origin, within which Eq. (43) is valid. The imaginary part of $K_{\perp_1}$ can be ignored inside this range[35], but not outside it. Just as for the L.T.A. and L.D.A. approximations developed previously, no general expression can be given to specify the range of validity of the L.T.D. approximation.

In the particular case illustrated by Fig. 8, it appears that Eq. (43) is a good approximation when $|K_{//}| \lesssim 0.1$. The range of validity is somewhat larger for negative values of $K_{//}$ than for positive values. Hence an approximate analytic calculation of the potential, based on Eq. (43), should give better results upstream than downstream.

Because our iterative method for finding complex roots starts from the origin K = 0, we must assume that the electrostatic waves what were responsible for the irregular oscillations of the potential in the case of a cold drifting magnetoplasma are damped by thermal processes. In other words, the imaginary part of $K_{\perp_1}$ is assumed to be much greater than its real part along the corresponding branches of the dispersion curve. These branches occur outside the range $(\Omega-1) < \kappa_{//} < \Omega$, which contains the least-damped ones (Fig. 5.a.). The definitions adopted in section II for the normalized wavenumbers involve $K_{//} = (r_L/\ell)\ \kappa_{//}$, so these branches occur for negative $K_{//} < (\Omega-1)\ r_L/\ell$ and for positive $K_{//} > \Omega\ r_L/\ell$. Since the limits of these ranges depend both on the normalized frequency Ω and on the ratio r_L/ℓ, the same must be true of the range of validity of the above assumtion. Again, it seems impossible to give a general expression to specify this range.

ANALYTIC CALCULATION OF THE POTENTIAL

The angular shift of the resonance cone due to field-aligned drift in a Maxwellian magnetoplasma has been calculated analytically by Kuehl. He did this by expressing the potential created by an alternating point charge as a power series in the variable $\varepsilon_v = R_\perp^{1/3} |\alpha|^{-2/3} \gamma \ell / r_L$, and by assuming only the first-order terms, on the assumption that $\varepsilon_v << 1$, i.e. that $r_\perp << \alpha^2\ r_L^4/\gamma^3\ \ell^3$. Then he calculated approximately the new value of the variable z_T for which the magnitude of the potential is maximum, namely $z_T = 1.800 + 0.906\ \varepsilon_v$; remember, from its definition by Eq. (16), that z_T is proportional to the angular drift of the resonance at fixed frequency.

In the case where the angle is kept fixed and we sweep the frequecy, it is more convenient to use the following expression for z_T near the resonance frequency :

$$z_T \approx R^{2/3}\ |\alpha|^{-1/3} \cos\beta\ \sin^{-1/3}\beta\ \Omega_c^{-1}\ (1-\Omega_c^2)^{-1}(\Omega-\Omega_c) \qquad (44)$$

Hence, the resonance frequency in a stationary Maxwellian plasma is

$$\Omega_o \gtrsim \Omega_c + 1.8\ \mathrm{sgn}(\alpha)\ R^{-2/3}\ |\alpha|^{1/3}\ \cos^{-1}\beta\ \sin^{1/3}\beta\ \Omega_c\ (1 - \Omega_c{}^2) \qquad (45)$$

Like the angular shift at fixed frequency, the resonance frequency shift $\Omega_0 - \Omega_c$ is proportional to $r_L{}^{2/3}$, and so to $T_e{}^{1/3}$.

In the presence of field-aligned drift, there is an additional shift which changes its sign when the emitting and receiving electrodes are interchanged. As in section IV, the resonance frequency will be called Ω_{+_0} when the receiver is upstream, and Ω_{-_0} when it is downstream from the transmitter. The average of these two frequencies is still Ω_0. Experimentally, one measures their difference

$$\Delta\Omega = \Omega_{+_0} - \Omega_{-_0} \gtrsim 1.812\ |\alpha|^{-1/3} R_\perp{}^{-1/3} \Omega_c (1-\Omega_c{}^2) \mathrm{tg}\beta\ \gamma \ell / r_L \qquad (46)$$

where α and γ are calculated at the frequency $\Omega = \Omega_c$. This <u>differential shift</u> is proportional to $\ell / r_L{}^{2/3} r_\perp{}^{1/3}$, and so to the ratio $V_{//}/v_{th}{}^{2/3}(r_\perp \omega_b)^{1/3}$

By following Kuehl's method, it is easy to calculate the same parameters Ω_0 and $\Delta\Omega$ in the other limit where $r_\perp >> \alpha^2\ r_L{}^4/\gamma^3\ \ell^3$. Downstream from the transmitter, the use of Eq. (43) for $\kappa_{\perp_1} = K_{\perp_1} \ell / r_L$ leads to a new integral for the potential :

$$\psi_+(\Omega,\underset{\sim}{\rho}) \underset{\sim}{\propto} i\frac{\rho}{2}\ \frac{1-\Omega^2}{\Omega_T{}^2-\Omega^2}\left[\frac{2\ i}{\Pi \rho_\perp \mathrm{cotg}\beta_c}\right]^{1/2} \int_0^\infty \exp\left\{ i\left[(\rho_{//} - \rho_\perp \mathrm{cotg}\beta_c)\kappa_{//} - \rho_\perp \gamma \kappa_{//}{}^2 - \rho_\perp \frac{r_L{}^2}{\ell^2}\ \kappa_{//}{}^3 \right] \right\} \kappa_{//}{}^{-1/2} d\kappa_{//} \qquad (47)$$

By series expanding the exponential containing the thermal correction term $- i\alpha\rho r_L{}^2\ K_{//}{}^3/\ell^2$, this expression can be rewritten as

$$\psi_+(\Omega,\underset{\sim}{\rho}) \underset{\sim}{\propto} - (8\Pi \mathrm{cotg}\beta_c)^{-1/2} \rho_\perp{}^{-3/4} \gamma^{-1/4} \sum_{n=o}^{\infty} \frac{\varepsilon_T{}^n}{n!} \frac{d^3 \Phi_+(\zeta_+)}{d\zeta_+{}^{3n}} \qquad (48)$$

where $\Phi_+(\zeta_+)$ is the function defined in section IV and $\varepsilon_T = \rho_\perp^{-1/2}\gamma^{-3/2}\alpha r_L^2/\ell^2$. Assuming $\varepsilon_T \ll 1.$, i.e. $r_\perp \gg \alpha^2 r_L^4/\gamma^3\ell^3$, we may retain only the first two terms of the series. From numerical calculations of Φ_+ and of its derivatives, together with a series expansion about the value $\zeta_+ = 2.199$ for which $|\Phi_+|$ is maximum, we find that the maximum magnitude of the potential occurs when $\zeta_+ = 2.199 + 0.128\ \varepsilon_T$. The analytic calculation of the potential ψ_- upstream from the transmitter is similar ; its magnitude is maximum for $\zeta_- = 2.199 - 0.128\ \varepsilon_T$. In each of these two formulas, the constant term, which has been derived already in section IV, represents the main effect of the drift motion : the second term represents the smaller additional effect of the thermal motion. Together, these formulas show that the differential shift in resonance frequency due to the drift motion, $\Delta\Omega = \Omega_{+_0} - \Omega_{-_0}$, is not affected by thermal motion while the average resonance frequency $(\Omega_{+_0} + \Omega_{-_0})/2$ which we shall now call Ω_a, is

$$\Omega_a \sim \Omega_c + 0.128\ \Omega_c\ (1 - \Omega_c^2)\ \rho_{//}^{-1}\ \gamma^{-1}\ \alpha\ r_L^2/\ell^2 \qquad (49)$$

Thus the average resonance frequency is shifted proportionally to the ratio r_L^2/ℓ - and so to T_e - due to the thermal motion ; while the differential shift in resonance frequency due to the drift is proportional to $V_{//}^{1/2}$, like in the cold-plasma case.

Before confronting these approximate results with the numerical results from our computer programme, we should point out some peculiarities of this analytic approach devised by Kuehl. His first step is to approximate the least-damped root of the dispersion equation. The errors that this involves have been discussed in the preceding subsection. The second step is to introduce a reference function by taking into account only one major effect, either that of the thermal motion or that of the drift motion. In so doing, the asymptotic expansion of the Hankel function is used in such a way that, when one calculates the potential, one cannot recover the case of the cold stationary magnetoplasma : note that when $R \to \infty$ (corresponding to $T \to 0$) in Eq. (15), or when $\rho \to \infty$ (corresponding to $V_{//} \to 0$) in Eq. (38), senseless results are obtained.

Moreover, the argument of this reference function is approximated near the resonance angle or frequency, and more errors are introduced thereby. The third step consists of expressing the potential as a power series in a parameter that takes account of the minor effect. The two infinite series obtained by starting from the one or the other reference function are strictly equivalent and include a coupling between the thermal and drift effects. Then, in a final set of approximations, the treatment of this coupling is simplified by truncating the series which amounts to ignoring the influence of the minor on the major effect, but not the converse. The errors committed at these successive steps of the analytic calculations can either reinforce or cancel one another, so it would be difficult to obtain any simple and global criterion of validity of all the approximations by comparison between the final approximate results and the exact numerical results.

NUMERICAL CALCULATION OF THE POTENTIAL

It is easy to modify our computer programme for calculating the potential created by an alternating point charge in a Maxwellian magnetoplasma, so as to introduce a field-aligned drift. In Eq. (4) for α_n, the term involving the ratio ℓ/r_L is now non-zero, and the numerical integration of Eq. (5) must now be performed from $-\infty$ to $+\infty$ since $K_{\perp_1}(K_{//}) \neq K_{\perp_1}(-K_{//})$. Limiting ourselves to the case where only the excitation frequency is varied, we shall present one example of a numerical calculation of the potential with Ω varying from 0 to 1., before focussing our attention on the resonance-frequency shift due to the plasma drift.

Fig. 9 shows the numerically-calculated frequency variations of the magnitude and phase of the potential at each of two fixed points, at equal distances from the source but in opposite directions. The parameter values are as given in the figure caption. At frequencies greater than the resonance frequency, all the curves shows an interference structure which is a thermal effect. In the amplitude curves, this structure is not sufficiently pronounced to produce actual maxima and minima, but such extrema appear distincly in the phase curves. The relative smoothness of the curves for ψ_- leads us to think that the interference structure due to the drift is damped by the thermal motion. The remaining - and most important -

effect of the drift is to shift the resonance frequency : in Fig. 9, the differential shift $\Delta\Omega$ is 0.522 while the approximate formulas (40) and (46) give 0.1185 and 0.0303 respectively. Since $r_\perp$ = 1.2 m and $\alpha^2 r_L{}^4/\gamma^3 \ell^3$ = 1.17 m, we are roughly in the intermediate range where neither of the approximate formulas is valid. Thus we have here a case where the exact differential shift due to the drift lies between the asymptotic values given by the two analytic calculations, though this is no true in every case.

In fact, the drift effect is systematically underestimated by using the L.T.D. approximation for the least-damped root of the dispersion equation, but this basic inadequacy is subsequently attenuated by the further approximations made in the analytic calculation of the resonance frequency shift. In Fig. 10, the variations of the differential frequency shift $\Delta\Omega$ are graphed versus ℓ in the case where Ω_p = 5., r = . 8 m and β = 30° or 150°, for R = 30, 50 and 100, and also for R = ∞ which is the cold-plasma case. The solid curves show the variations calculated numerically with our complete computer programme, in which the least-damped root $K_{\perp 1}$ of Eq. (2) is determined by the iterative complex-root-finding method ; the dashed curves are the approximations, obtained from Eq. (46) when R is finite and from Eq. (40) when R is infinite. In this example, Eq. (46) gives a differential frequency shift $\Delta\Omega$ less than the exact value when R is large and greater than the exact value when R is small. We note that this result is consistent with the L.T.D. approximation which is valid when the distance is both large enough to justify the use of the low-temperature approximation and small enough to satisfy the condition $r_\perp \ll \alpha^2 r_L{}^4/\gamma^3 \ell^3$. On the other hand, the exact values of $\Delta\Omega$ vary more or less linearly with ℓ, even for large values of R ; this result disagrees with the prediction of Eq. (40), which is plotted as the dashed curve labelled R = ∞, according to which $\Delta\Omega$ should be proportional to $\ell^{1/2}$. Generally speaking, Eq. (40) seems to be more of theoretical than of practical interest since the conditions for it to be applicable do not occur in the experimental situations that we envisage. In this example, where β = 30° (or 150°), Kuehl's formula for $\Delta\Omega$ would be useful for data analysis, but we use of the numerical values for $\Delta\Omega$ would improve the accuracy.

This rough agreement between the approximate and the exact values of $\Delta\Omega$ for $\beta = 30°$ may be better or worse at other values of this angle. Fig. 11 shows the differential shift $\Delta\Omega$ calculated for $\Omega_p = 5.$, $R = 100$ and $\ell/r_L = 0.1$ ($r = 0.8$ m) when β varies from 0° to 90°. The accompanying variation of the resonance frequency is given by the curve of β_0 in Fig. 3. The approximate values from Eq. (46) are graphed as the dashed curve and the exact values as the solid curve ; the composite curve shows the values of $\Delta\Omega$ derived from Eq. (40). Because of the factor $|\alpha|^{-1/3}$ in Eq. (46), Kuehl's approximation for $\Delta\Omega$ becomes infinite at the angle $\beta_\alpha = 44.57°$ where $\alpha = 0$; this is the resonance angle for the frequency Ω_α (see Section III). This infinity does not appear in the numerical calculation : the exact curve has a smooth maximum for a value of β somewhat less than β_α. Obviously, in any attempt to detect the drift effect experimentally, one would choose to work in a range of β around this maximum. It is noteworthy that, in this range, neither of the analytic approximations for the differential frequency shift $\Delta\Omega$ is usable. We conclude that Kuehl's formula is inadequate for interpreting measurements of the lower oblique resonance frequency to obtain the field-aligned drift velocity.

VI. SUMMARY AND CONCLUSIONS

In this paper, the effect of field-aligned drift on the lower oblique resonance in a Maxwellian magnetoplasma has been investigated, both analytically and numerically, by taking account only of the least-damped root of the dispersion equation and neglecting collisions and ion motion.

Our analytic results complement those that have been published in the recent years, particularly by Kuehl. They are valid only when the characteristic length $\ell = V_{//}/\omega_b$ is much smaller than the distance to the point of observation and when the drift velocity is much smaller than a critical value which depends on the plasma parameters and on the parameters of the measuring instrument. It is found that the shift in the resonance and the interference-structure spacing due to the drift are proportional to the square root of the drift velocity. This is contradictory with the linear proportionality discovered by Kuehl when the drift velocity is much greater than this critical value but it seems not possible to relate these two results analytically.

On the contrary, our numerical results are available whatever the values of thermal and drift velocities may be :

i) for a warm stationary plasma, the characteristic parameters of the potential distribution (i.e. positions and magnitudes of the succesive maximas and minimas) obtained from our computer programme are sometimes in contradiction with those deduced by Kuehl and other authors.

ii) in a cold drifting plasma, our numerical results for the potential are similar to those of Storey and Pottelette, although in our case the plasma is of finite density and the source is motionless. By using the Fourier transform to calculate the potential numerically, we are able to identify the branches of the dispersion curve that are responsible for the irregular oscillations.

iii) in a warm drifting magnetoplasma, we must assume that these irregular oscillations are damped by thermal processes but it is thought that this assumption is not very restrictive. From the comparison between the analytical and numerical values of the differential shift due to the drift, we have shown that our computer programme improves the accuracy of the results significantly in physically realistic situations.

For diagnostic purposes, our computer programme should be useful for interpreting measurements of the potential created by an alternating point charge near the lower oblique resonance. Experimentally, the electrodes of the probe must be arranged so as to give the highest possible sensitivity, i.e. the largest variations of the characteristic parameters of the potential distribution (resonance angle or frequency and interference structure spacing) for given variations of the plasma parameters (electron density, temperature and drift velocity). With these conditions, the approximate formulas previously published are insufficiently accurate.

i) for electron density and temperature measurements, the distance between the two electrodes must be small enough to yield large interference structure and a large resonance. Because their accuracy decreases with decreasing distance, Kuehl's appropriate formulas become less and less useful as the experimental conditions improve.

ii) for field-aligned drift velocity measurements, the probe is most sensitive when the angle between the magnetic-field direction and the line joining the two electrodes is around 45°, in the typical conditions considered. Unfortunately, the differential resonance-frequency shift is predicted badly by the analytic formula in the vicinity of this angle, at which indeed the prediction diverges. Again, we conclude that our re-evaluation of the drift effect is indeed necessary when the experimental device is optimized for plasma diagnostics.

This work is a contribution to the study of the lower oblique resonance, a subject that has developed greatly in recent years. It completes the previously published results by suppressing some restrictive conditions on the plasma parameters ; however, it is itself limited and it can be followed up in many directions.

First, our computer programme is thought to be well suited for studying some secondary effects of physical interest in the context of the least-damped root approximation.

i) the effects of collisions have been experimentally analyzed by Singh and Gould[36]. A rough numerical experiment can be made easily by replacing, in the subroutine for solving the dispersion equation, the frequency ω by the term $\omega - i\nu$ where ν is a small relaxation collision frequency.

ii) the effects of ions have been studied analytically by Kuehl[37] and Burrell[38]. Their results can be usefully completed by a numerical calculation which requires a new subroutine for the dispersion equation.

iii) the effect of a sheath around the transmitting antenna in a drifting magnetoplasma can be analyzed roughly by following a suggestion of Storey[39]. In a idealized model, charge supplied to the transmitting monopole antenna by a sinusoidally-varying input current accumulates on the antenna if the sheath is capacitive but flows straight off it into the plasma, where it joins the drift motion, if the sheath is resistive. Thus the present calculations would concern a capacitive sheath, whereas it is necessary to multiply the kernel of the integral in Eq. (5) by $(1 - K_{//}\, \ell/\Omega r_L)^{-1}$ to take into account the motion of the point charge in the case where the sheath is resistive.

Secondly, the electromagnetic effects also can be studied in the context of the least-damped root approximation. Lewis and Keller[40] have derived the dispersion equation for electromagnetic waves in a Maxwellian magnetoplasma ; this equation is available in the form of a computer subroutine thanks to Muldrew[21]. By considering only the least-damped root of his equation, it seems possible to numerically calculate the electric field radiated by a small dipole antenna. Theoretically, such a calculation would extend the pioneer calculation of Fisher and Gould[9] to the case were the magnetic field is finite, without having to make the quasi-static approximation used by Kuehl[12]. Experimentally, the numerical knowledge of the coupling between two dipole antennas would permit us to study the relative ments of different layouts of these antennas, in order to improve the sensitivity of the probe for plasma diagnostics.

Thirdly, new numerical calculations would be made to complete our theoretical knowledge of the lower oblique resonance. A first step would consist of taking account of all the roots of the dispersion equation for the electrostatic waves. To do this, it seems necessary to calculate the kernel of the integral in Eq. (5) numerically by integration along the positive part of the real K - axis rather than to use the residue theorem, as we have here when taking account only of the least-damped root. Such a numerical calculation along the real axis (or along a deformed path with no roots of the dispersion equation between it and the real axis) would be extended, in a second step, to the case where the magnetoplasma is non-Maxwellian. This research would be very useful because, when the drift velocity increases, the electron velocities probably have a non-Maxwellian distribution, especially in space plasmas.

ACKNOWLEDGEMENTS

This study was undertaken at the suggestion of Dr. L.R.O. STOREY and I am particularly grateful for all the advice that he gave me unsparingly during the course of it. Thanks are also due to D.B. MULDREW for providing me with a copy of his programme that computes the roots of the kinetic dispersion relation, and to C. BEGHIN for stimulating discussions.

This work was sponsored by the National Centre for Space Studies (C.N.E.S.). It was undertaken in connexion with the participation by the C.R.P.E. in the West-German PORCUPINE programme of rocket experiments on auroral physics during the International Magnetospheric Study.

FOOT NOTES

1. R.K. FISHER and R.W. GOULD, Phys. Rev. Letters 22, 1093 (1969).

2. A. GONFALONE, Le Journal de Physique 33, 521 (1972).

3. K.G. BALMAIN, Electronics Letters 9, 312 (1973).

4. K.H. BURRELL, Phys. Fluids 18, 1716 (1975).

5. H.C. KOONS, D.C. PRIDMORE-BROWN and D.A. Mc PHERSON, Radio Science 9, 541 (1974).

6. A. GONFALONE, Radio Science, to be published.

7. E. MICHEL, C. BEGHIN, A. GONFALONE and I.F. IVANOV, Annales de Geophysique 31, 463 (1975).

8. R. POTTELETTE and G. CISSOKO, in Space Research XIV, 375 (1974).

9. R.K. FISHER and R.W. GOULD, Phys. Fluids 4, 857 (1971).

10. N. SINGH and R.W. OGULD, Phys. Fluids 16, 75 (1973).

11. H.H. KUEHL, Phys. Fluids 16, 1311 (1973).

12. H.H. KUEHL, Phys. Fluids 17, 1275 (1974).

13. J.M. CHASSERIAUX, Phys. Fluids 18, 866 (1975).

14. O. STOREY and R. POTTELETTE, Compt. Rend. 273, 101 (1971).

15. R. POTTELETTE, Annales de Geophysique 29, 201 (1973).

16. N. SINGH, Phys. Fluids, to published. This author finds that the drift effect is more important than the thermal effect in a uniaxial magnetoplasma if the field aligned drift velocity is greater than a critical value which depends only on the thermal velocity and on the resonance-cone angle.

17. K.G. BALMAIN, IEEE Trans. Antennas Propagation AP-12, 605 (1964).

18. J.M. CHASSERIAUX, Annales de Geophysique 27, 329 (1971).

19. T.H. STIX, The Theory of Plasma Waves (Mc Graw-Hill, New York, 1962) chap. 9, p. 225.

20. B.D. FRIED and S.D. CONTE, The Plasma Dispersion Function (Academic Press, Inc., New York, 1961).

21. D.B. MULDREW and M.F. ESTABROOKS, Radio Science 7, 579 (1972).

22. M. ABRAMOWITZ and I. SEGUN, Handbook of Mathematical Functions (Dover Publications, Inc., New York, 1968), Chap. 25, p. 878.

23. J.A. WARD, J. Assoc. Computing Machinery 4, 148 (1957).

24. L.N.G. FILON, Proc. Roy. Soc. Edinburgh 49, 38 (1929).

25. A sketch of the function α is given in Fig. 2 of Ref. 5 ; its sign is plotted in the (Ω_p, Ω) plane in Fig. 4 of Ref. 11.

26. D.B. MULDREW and A. GONFALONE, Radio Science 9, 873 (1974). Dispersion curves for homogeneous electrostatic waves near the lower oblique resonance are shown in Fig. 4 and 7.

27. Obviously, this conclusion also applies to the formulas given by BURRELL (Réf. 4) and CHASSERIAUX (Réf. 13) which are similar to those of KUEHL.

28. See Fig. 4 of Réf. 6 In his interpretation of the data shown in this figure, the author has mistakenly deduced the electron density from the cold plasma theory.

29. N. SINGH, IEEE Trans. Antennas Propag. AP-20, 77 (1972). This work is concerned with the dispersion equation for electromagnetic waves in a cold uniaxial plasma drifting along the magnetic field.

30. When the frequency of the alternating point charge is fixed, the potential distribution derived from similar calculations has the following characteristics : doxnstream from the point source, the resonance cone becomes narrower and a regular interference structure lies inside it while irregular oscillations appear outside it ; upstream from the point source, the resonance cone becomes wider and a regular interference structure lies outside it.

31. Because of the term - t in the exponent, the integrand vanishes everywhere in the right half plane when $|t| \to \infty$. Therefore, we way deform the contour of integration to make it lie entirely on the positive real axis.

32. See Ref. 22, p. 253.

33. The analytic formulas A.I. 23 and A.I. 24 of Ref. 15 only concern the case where the receiver is upstream from the transmitter and the numerical coefficient π is deduced directly from the phase variation of $Z^{\circ}(\chi)$ in Fig. 17 of Ref. 15. In fact, this phase variation depends critically on the value τ_o of Ref. 15 which has been taken arbitrarily as 3.3 This is would not be correct to interpret the slight discrepancies between the formulas given in Ref. 15 and those in the present paper as having physical significance.

34. From analytic considerations, we infer that the drift effect is more important than the thermal effe when the drift velocity is greater than the critical value $V_c = (\alpha^2/4\omega_b\gamma^3 r_\perp)^{1/3} v_{th}^{4/3}$

35. In neglecting the imaginary part of K 1 in Eq. (43), one fails to take account of the fact that $\mathrm{Im}\, K_{\perp 1}(K_{//}) > \mathrm{Im}\, K_{\perp 1}(-K_{//})$ which means physically that the inhomogeneous electrostatic waves are more heavily damped when they are propagated against the plasma flow than when they go along with it.

36. See Ref. 10, Fig. 3.

37. H.H. KUEHL, Phys. Fluids 17, 1636 (1974).

38. K.H. BURRELL, Phys. Fluids 18, 897 (1975).

39. L.R.O. STOREY, private communication.

40. R.M. Levis and J.B. KELLER, Phys. Fluids 5, 1248 (1962).

FIGURES CAPTIONS

Figure 1. Typical behaviour of the least-damped root $K_{\perp 1}$ of the dispersion equation, as a function of real $K_{//}$ for various fixed values of Ω, with $\Omega_p = 5$: ▬▬ exact values of he $K_{\perp 1}$; ——— approximate values derived from Eq. (12) ; ▬ · ▬ · ▬ cold plasma approximation ; ····· exact values of Im $K_{\perp 1}$.

Figure 2. Normalized magnitude of the potential of an alternating point change, for $\Omega_p = 5$, $\Omega = 0.5$ and R = 100. The solid curve was obtained by numerical calculation and the dashed curve from Eq. (15).

Figure 3. The angles β_n (n = 0, 1, 2) of the successive maxima in the potential as functions of Ω, for $\Omega_p = 5$ and R = 100 ▬▬ exact values ; ····· approximate values : from Eq. (11) and (12) ; ▬ · ▬ · ▬ cold-plasma approximation.

Figure 4. The angles marked in Fig. 2, plotted as function of R, for $\Omega = 0.5$.

Figure 5.a. Numerically-calculated value of the chosen root $\kappa_{\perp 1}$ of the dispersion equation as a function of real $\kappa_{//}$ for $\Omega = 0.5$ and $\Omega_p = 5$: ▬▬ values of Re ($\kappa_{\perp 1}$) ; ····· values of Im ($\kappa_{\perp 1}$) ; ▬ · ▬ · ▬ stationary plasma case (where $\kappa_{\perp 1}$ is purely real).

Figure 5.b. The region of Fig. 5.a. around the origin is shown here on a larger scale. $\kappa_{\perp 1}$ is purely real and the dashed line shows the approximation of Eq. (21).

Figure 6.a. Normalized magnitude of the potential created upstream from an alternating point charge for $\Omega_p = 5$, $\rho = 160$ and $\beta = 30°$; ▬▬▬ exact result. ▬▬▬▬ result obtained by partial integration of Eq. (19) from $\Omega-1$ to Ω.

Figure 6.b. Normalized magnitude of the potential created downstream from an alternating point charge for $\Omega_p = 5$, $\rho = 160$ and $\beta = 150°$; ▬▬▬ exact result. ▬▬▬▬ reslut obtained by partial integration of Eq. (19) from $\Omega-1$ to Ω.

Figure 7. The curve of $|\Phi_+(\zeta_+)|$ versus ζ_+, as computed from the series expansion of Eq. (36) when $|\zeta_+| < 4$, and from the asymptotic forms of Eq. (36.a) and (36.b) when $|\zeta_+| > 4$.

Figure 8. The least-damped root K_1 of the dispersion equation in a drifting Maxwellian magnetosplasma, as a function of real $K_{//}$, for $\Omega_p = 5.$, $\Omega = .5$ and $\ell/r_L = .25$: ▬▬▬ exact values of Re $K_{\perp 1}$; ▬▬▬▬ approximate values derived from Eq. (43) ; ▬▬▬·▬▬▬·▬▬▬ stationary cold magnetoplasma approximation ; ▪▪▪▪▪▪▪▪▪▪▪▪▪ exact values of Im $K_{\perp 1}$.

Figure 9. Variations of the magnitudes and of the phases of the normalized potentials ζ_+ and ψ_- for $\Omega_p = 5$, r = 2.4 m, β =30° and 150°, R = 90 and $\ell/r_L = .225$ ($V_{//} = 0.159\ v_{th}$).

Figure 10. Curves of the differential frequency drift $\Delta\Omega$ due to the plasma drift, versus ℓ for $\beta = 30°$, r = 0.8 m and R = 30,50 and 100 : ▬▬▬▬ complete numerical calculation ; ▪▪▪▪▪▪▪▪▪▪▪▪▪▪▪ use of Eq. (40) for R = ∞ and (46) for R = 30, 50 and 100.

Figure 11. Curves of $\Delta\Omega$ versus β for $\Omega_p = 5$, $\beta = 30°$, r= .8 m, R = 100 and $\ell/r_L = .1$: ▬▬▬▬ complete numerical calculation ; ▪▪▪▪▪▪▪▪▪▪▪▪▪▪▪▪▪▪▪ : use of Eq. (46) ; ▬▬▬·▬▬▬·▬▬▬ use of Eq. (40).

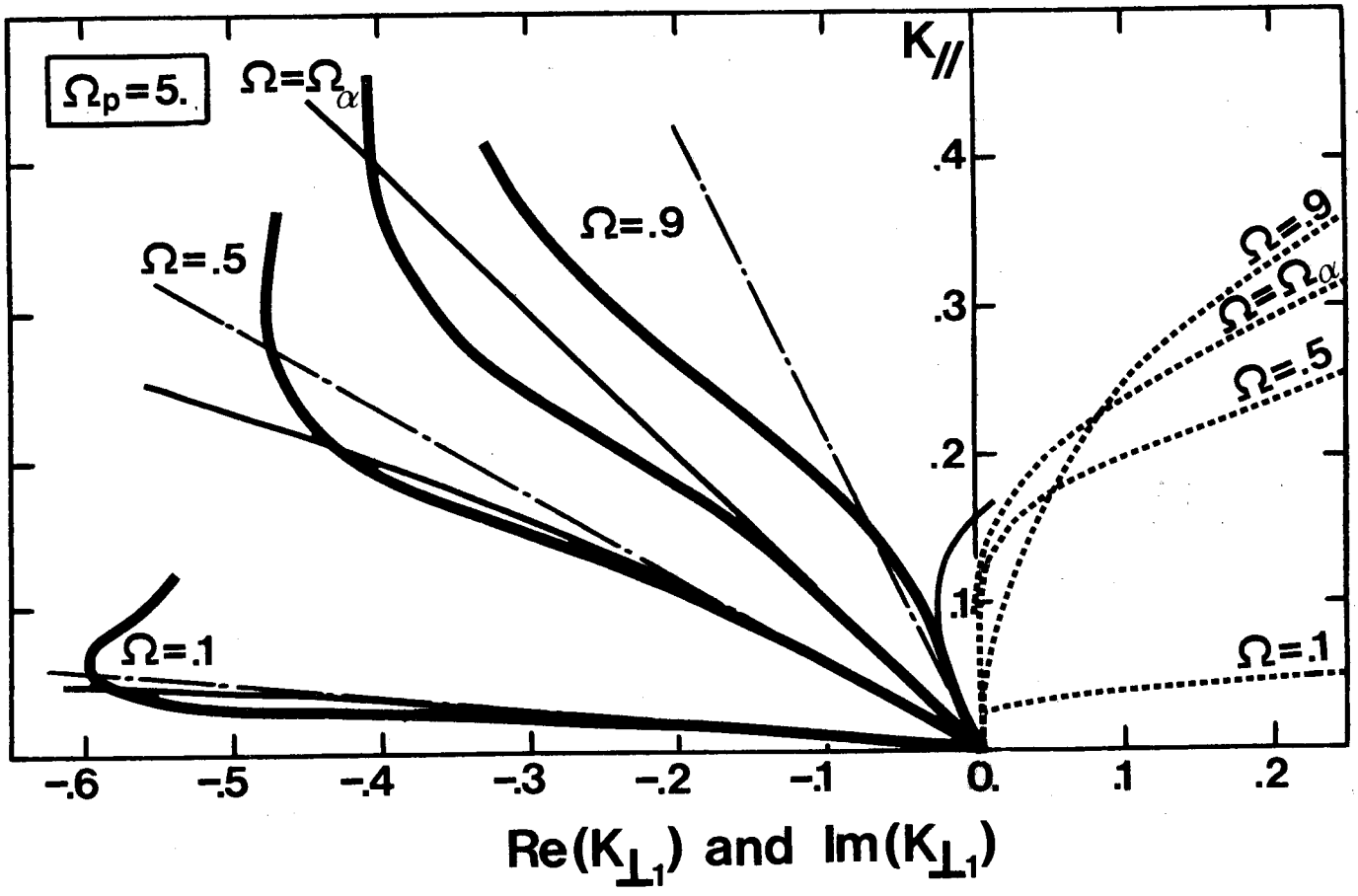
Ω_p=5.
$\Omega=\Omega_\alpha$
Ω=.9
Ω=.5
Ω=.1
$K_{//}$
.4
.3
.2
.1
Ω=.9
$\Omega=\Omega_\alpha$
Ω=.5
Ω=.1
-.6
-.5
-.4
-.3
-.2
-.1
0.
.1
.2
Re($K_{\perp_1}$) and Im($K_{\perp_1}$)

Figure 1.

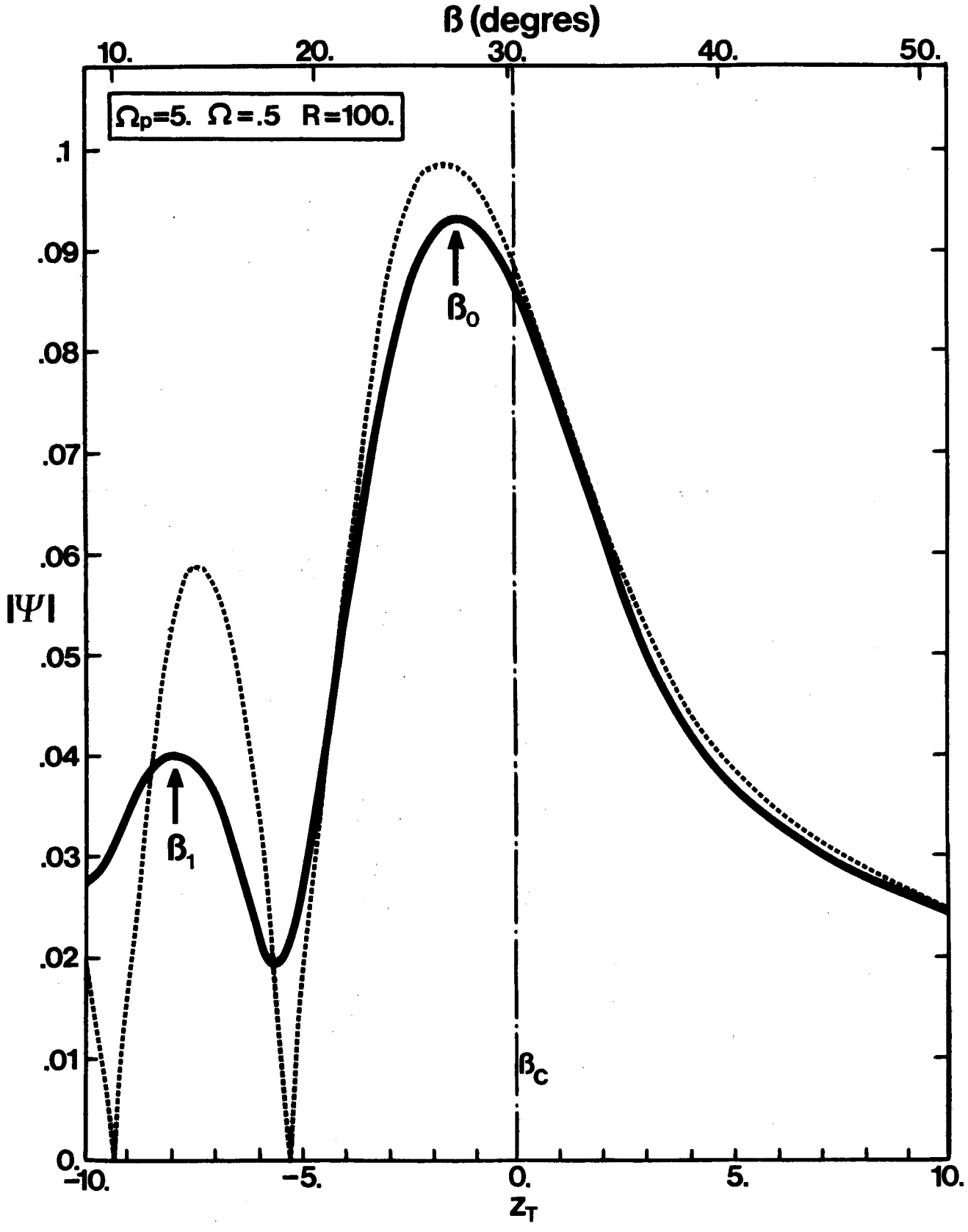
ß (degres)
10.
20.
30.
40.
50.
Ωp=5. Ω=.5 R=100.
.1
.09
.08
.07
.06
|Ψ|
.05
.04
.03
.02
.01
0.
ß0
ß1
ßc
-10.
-5.
0.
5.
10.
zT

Figure 2.

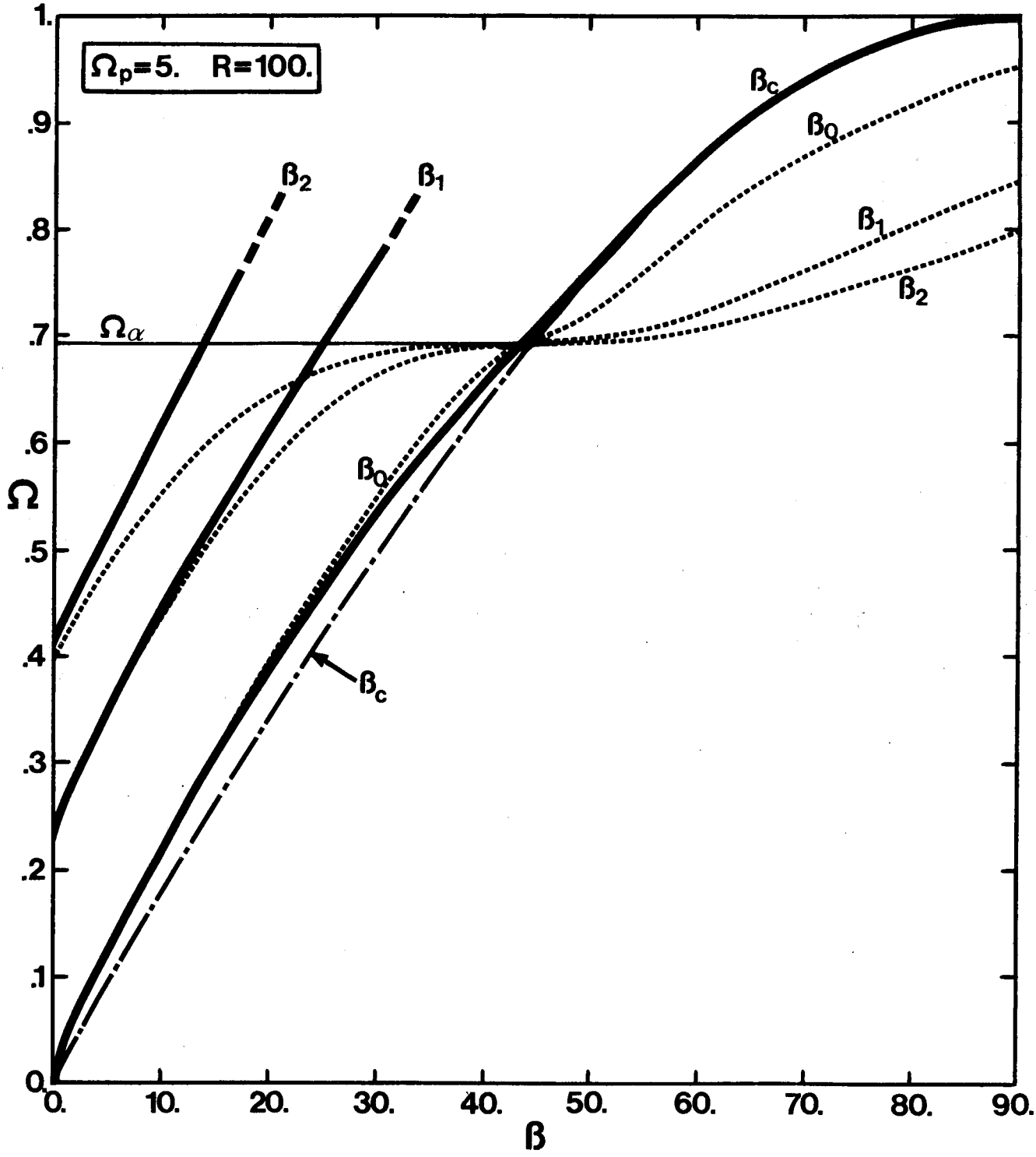
Ω_p=5. R=100.
β_c
β_0
β_2
β_1
β_1
β_2
Ω_α
β_0
β_c
Ω
1.
.9
.8
.7
.6
.5
.4
.3
.2
.1
0.
0.
10.
20.
30.
40.
50.
60.
70.
80.
90.
β

Figure 3.

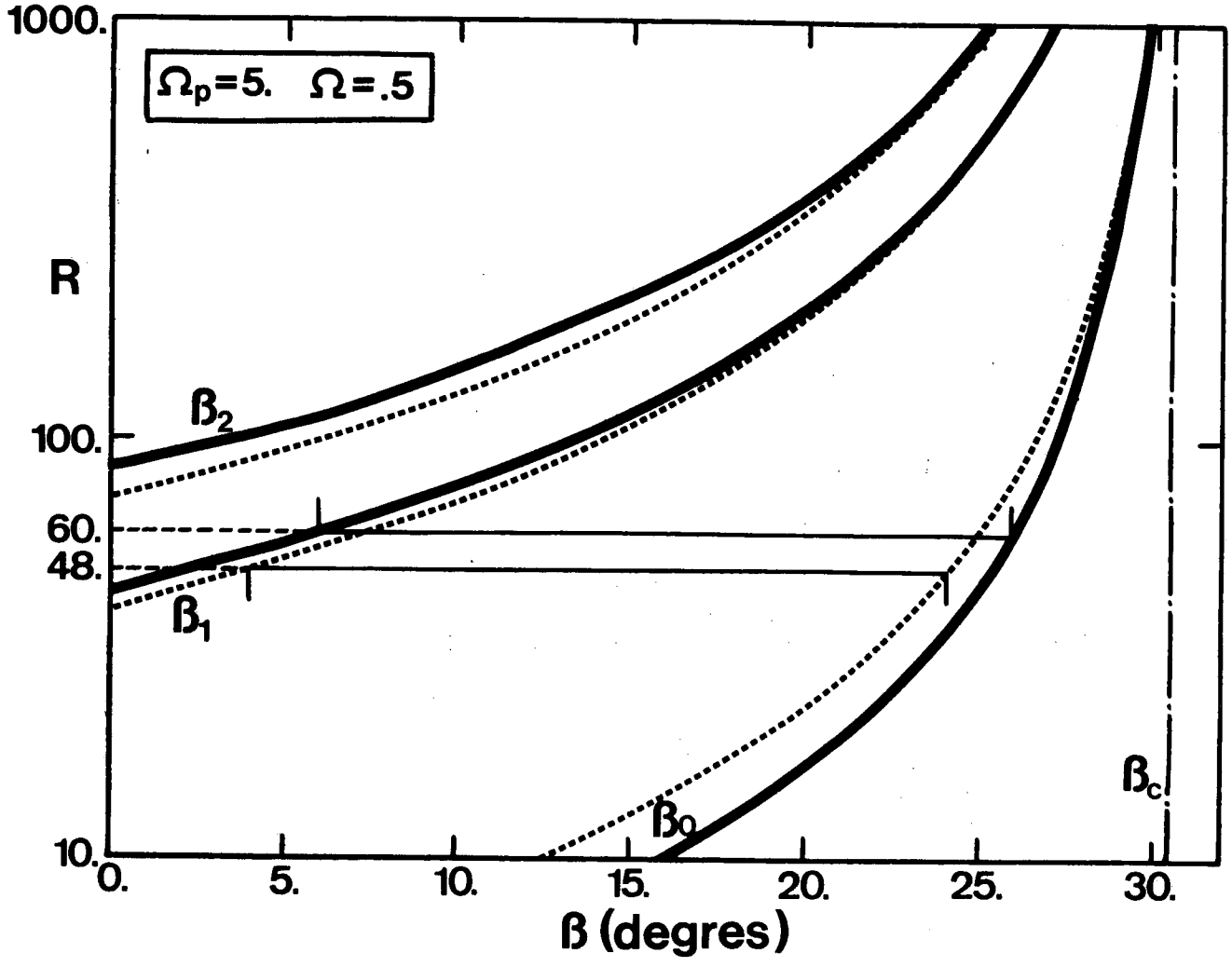
1000.
Ω_p=5. Ω=.5
R
100.
60.
48.
10.
β_2
β_1
β_0
β_c
0.
5.
10.
15.
20.
25.
30.
β (degres)

Figure 4.

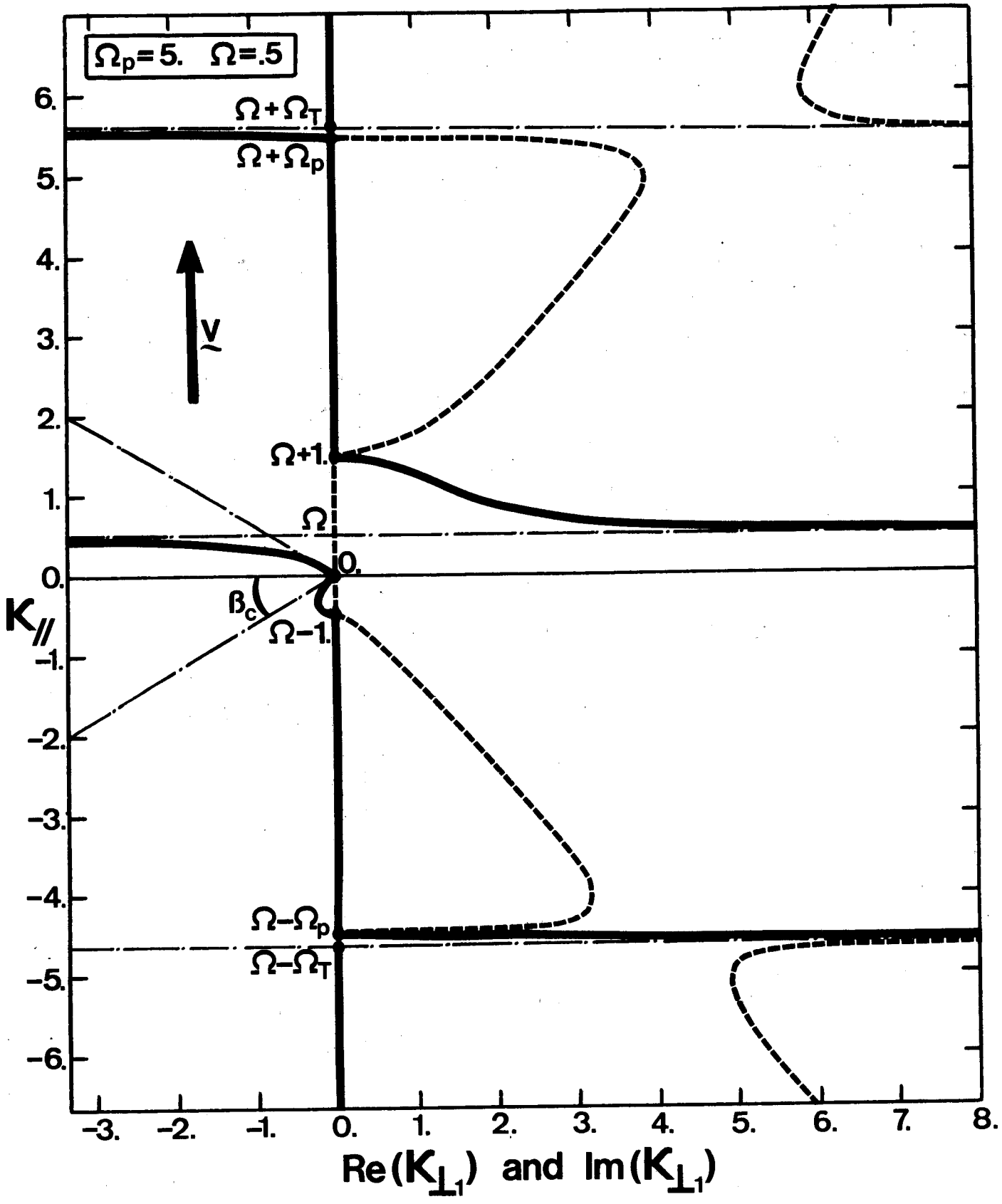
Ω_p=5. Ω=.5
$\Omega+\Omega_T$
$\Omega+\Omega_p$
V
Ω+1.
Ω
0.
β_c
Ω−1.
$\Omega-\Omega_p$
$\Omega-\Omega_T$
$K_{//}$
6.
5.
4.
3.
2.
1.
0.
−1.
−2.
−3.
−4.
−5.
−6.
−3.
−2.
−1.
0.
1.
2.
3.
4.
5.
6.
7.
8.
Re($K_{\perp_1}$) and Im($K_{\perp_1}$)

Figure 5.a.

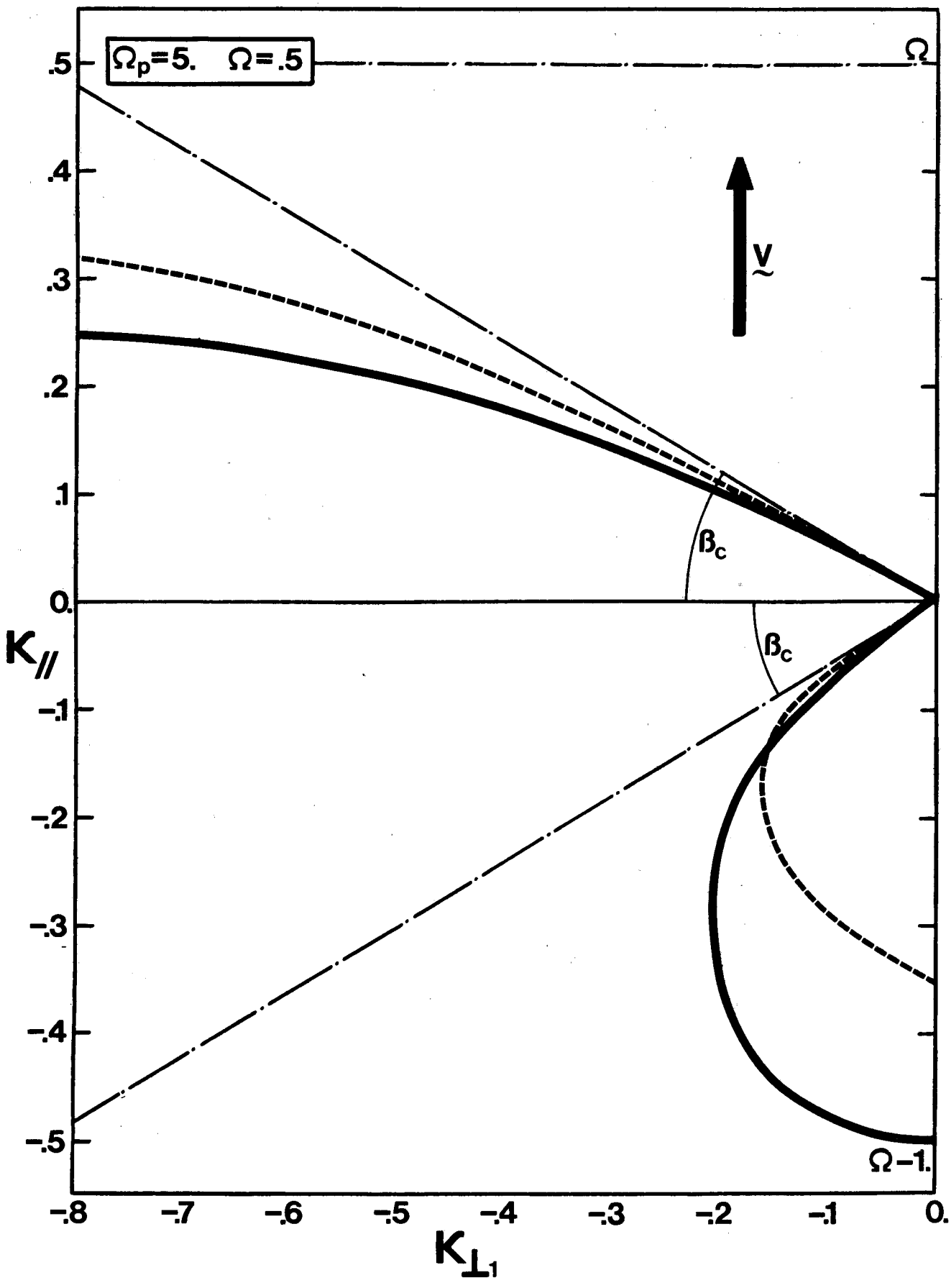
Ω_p=5. Ω=.5
Ω
V
β_c
β_c
$K_{//}$
$K_{\perp_1}$
Ω=1.
.5
.4
.3
.2
.1
0.
-.1
-.2
-.3
-.4
-.5
-.8
-.7
-.6
-.5
-.4
-.3
-.2
-.1
0.

Figure 5.b.

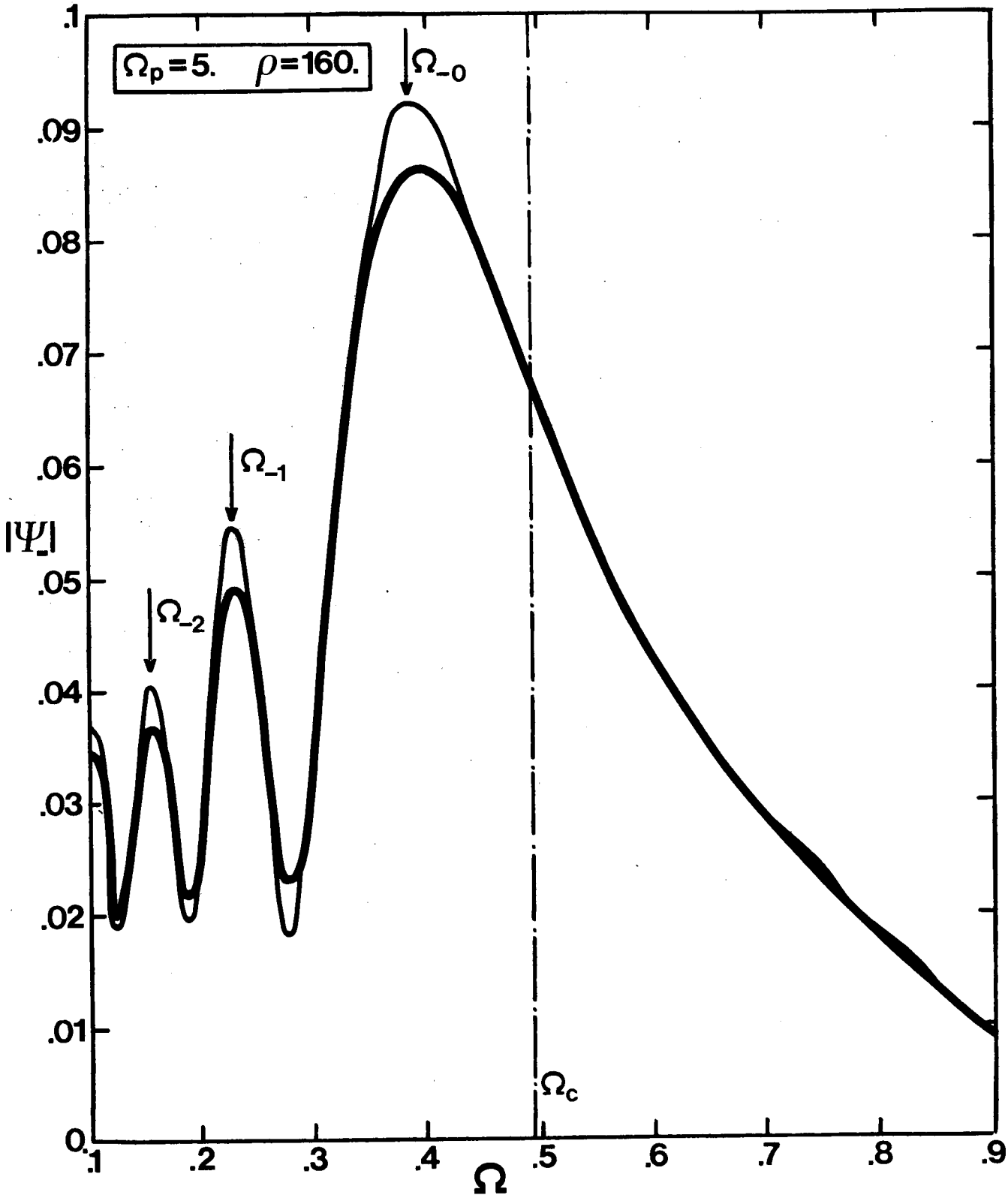
Ω_p=5. ρ=160.
Ω_{-0}
Ω_{-1}
Ω_{-2}
Ω_c
$|\Psi_-|$
Ω
.1
.09
.08
.07
.06
.05
.04
.03
.02
.01
0
.1
.2
.3
.4
.5
.6
.7
.8
.9

Figure 6.a.

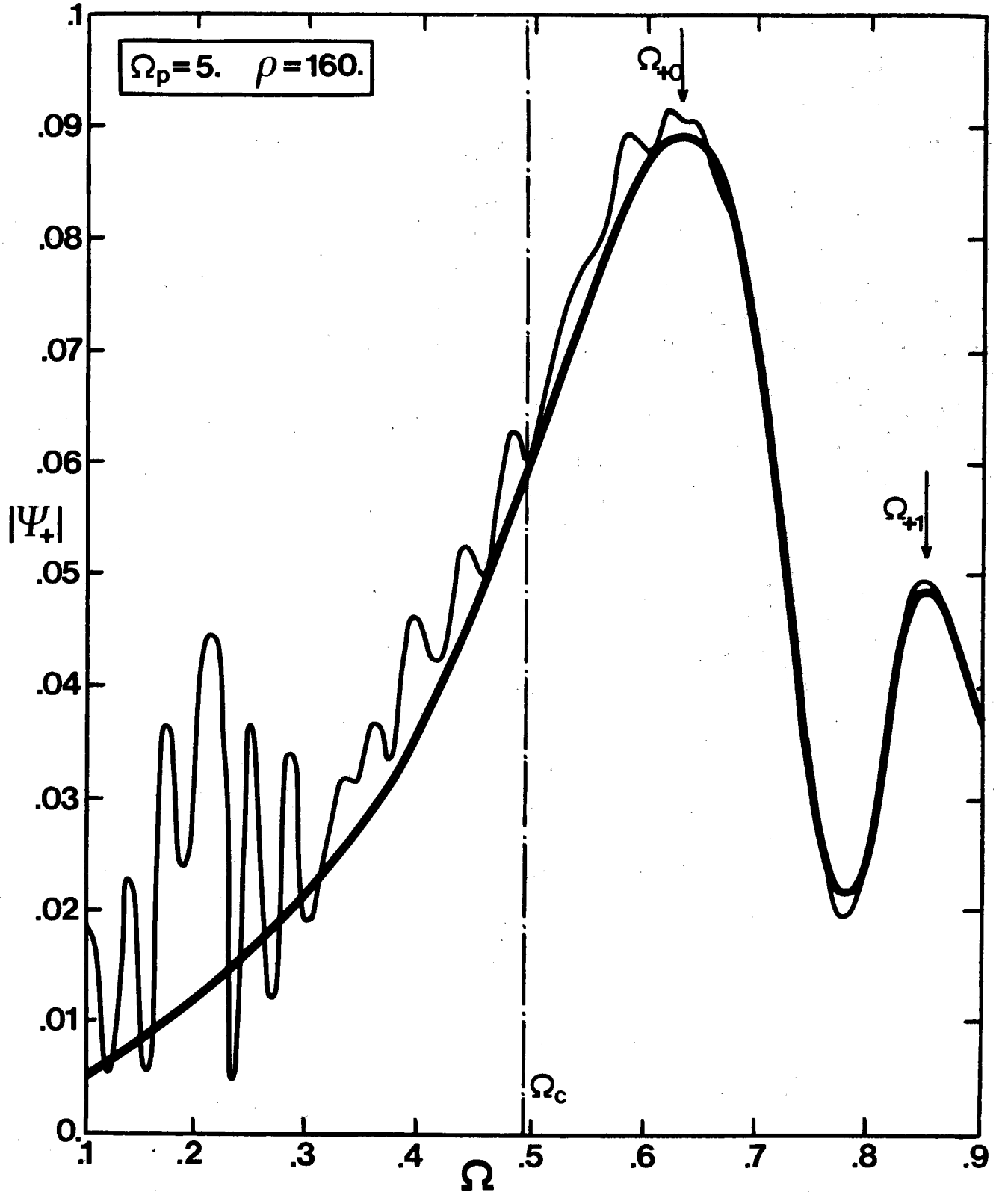
$\Omega_p = 5.$ $\rho = 160.$
Ω_{+0}
Ω_{+1}
Ω_c
$|\Psi_+|$
Ω
.1
.09
.08
.07
.06
.05
.04
.03
.02
.01
0.
.1
.2
.3
.4
.5
.6
.7
.8
.9

Figure 6.b.

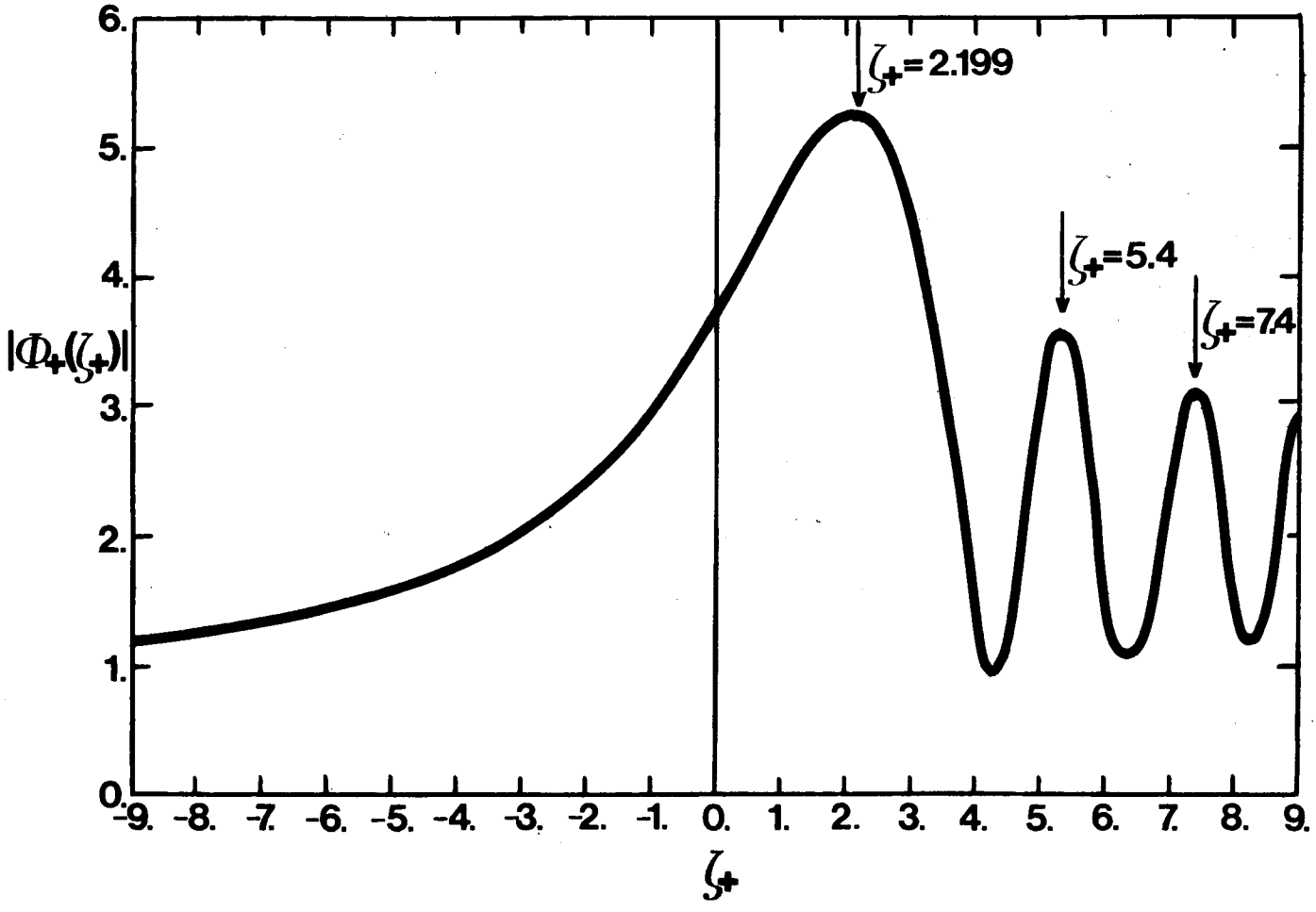
6.
5.
4.
3.
2.
1.
0.
$|\Phi_+(\zeta_+)|$
$\zeta_+=2.199$
$\zeta_+=5.4$
$\zeta_+=7.4$
-9. -8. -7. -6. -5. -4. -3. -2. -1. 0. 1. 2. 3. 4. 5. 6. 7. 8. 9.
ζ_+

Figure 7.

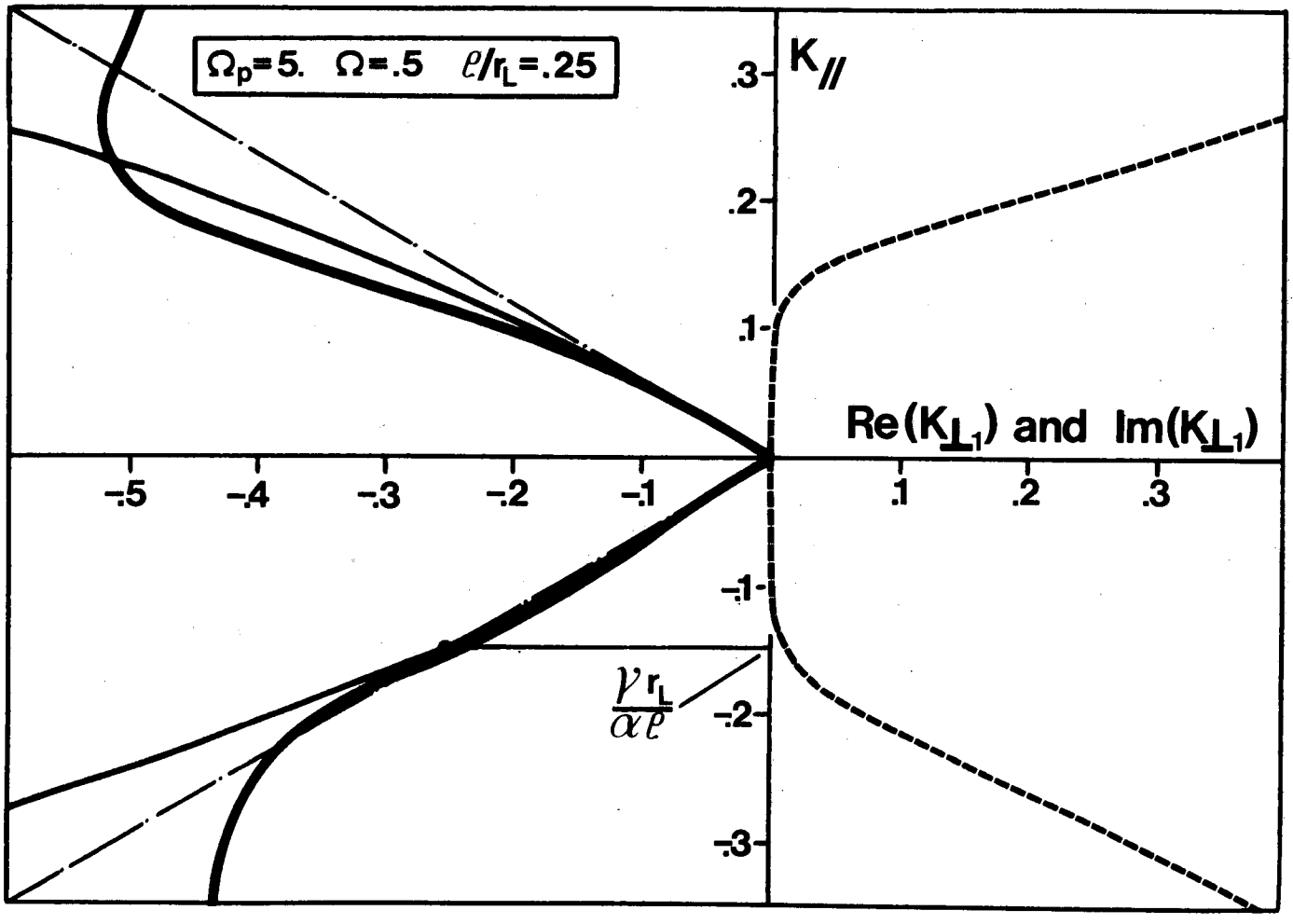
Ω_p=5. Ω=.5 ℓ/r_L=.25
$K_{//}$
.3
.2
.1
-.1
-.2
-.3
-.5
-.4
-.3
-.2
-.1
.1
.2
.3
Re($K_{\perp_1}$) and Im($K_{\perp_1}$)
$\frac{\nu r_L}{\alpha \ell}$

Figure 8.

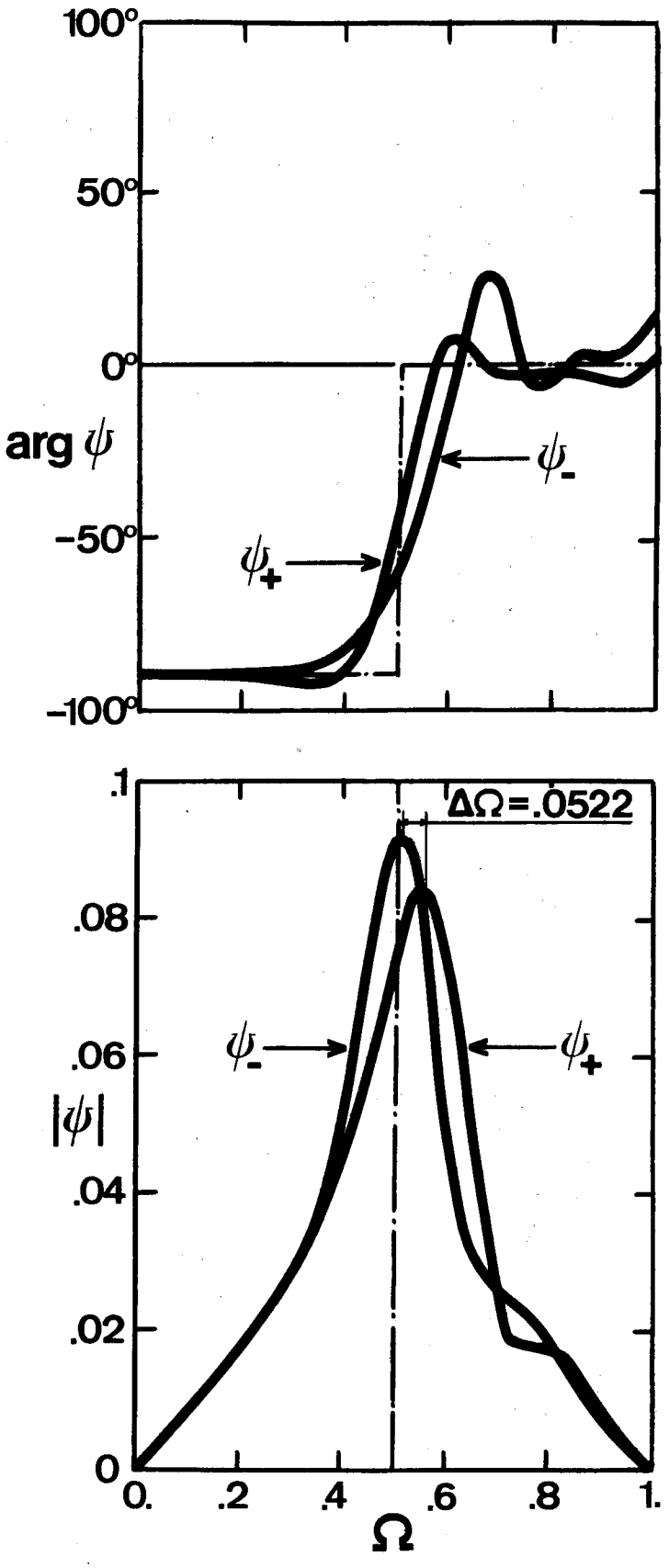

Figure 9.

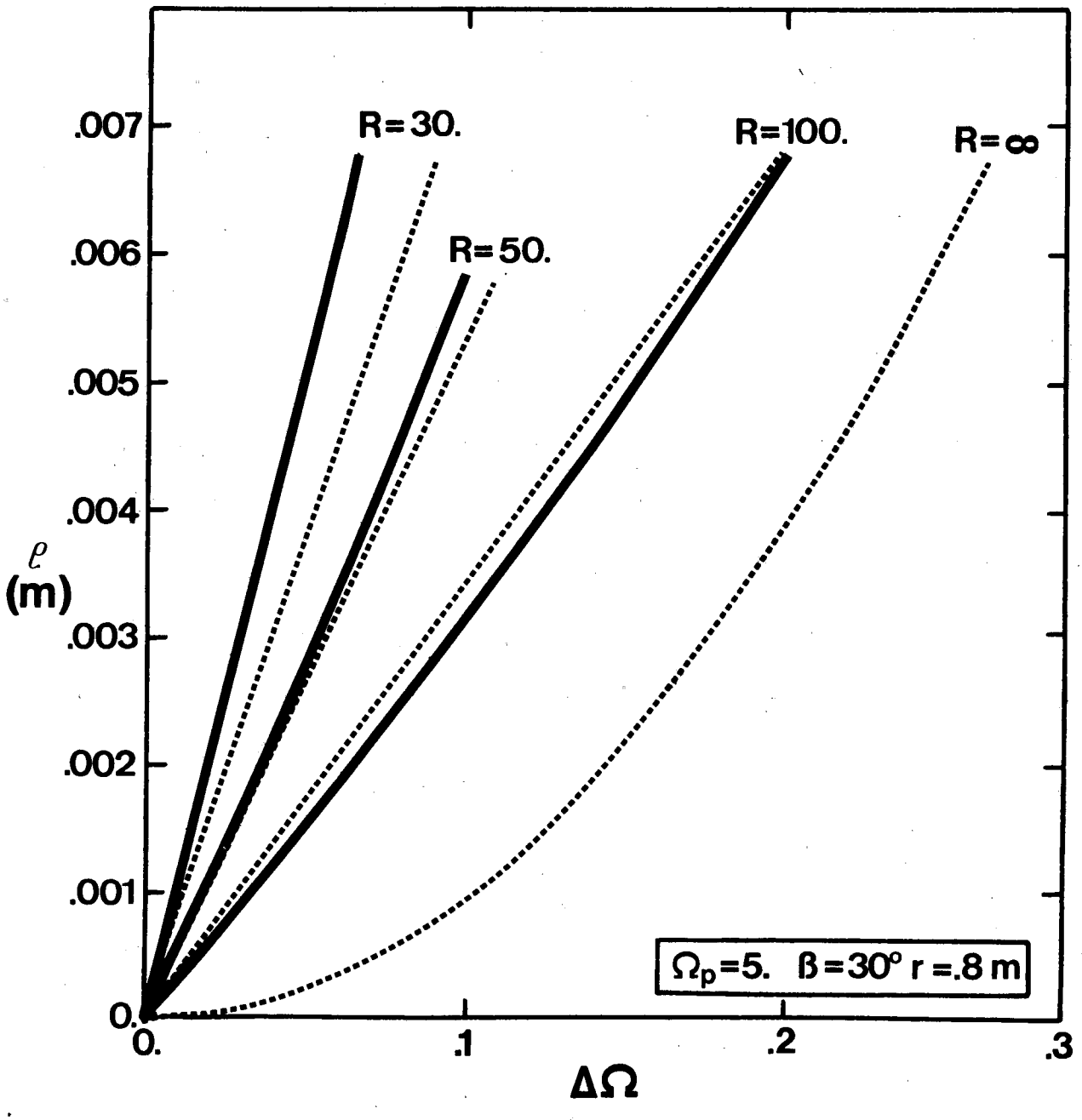
.007
.006
.005
.004
.003
.002
.001
0.
ρ
(m)
R=30.
R=50.
R=100.
R=∞
Ωp=5. β=30° r=.8 m
0.
.1
.2
.3
ΔΩ

Figure 10.

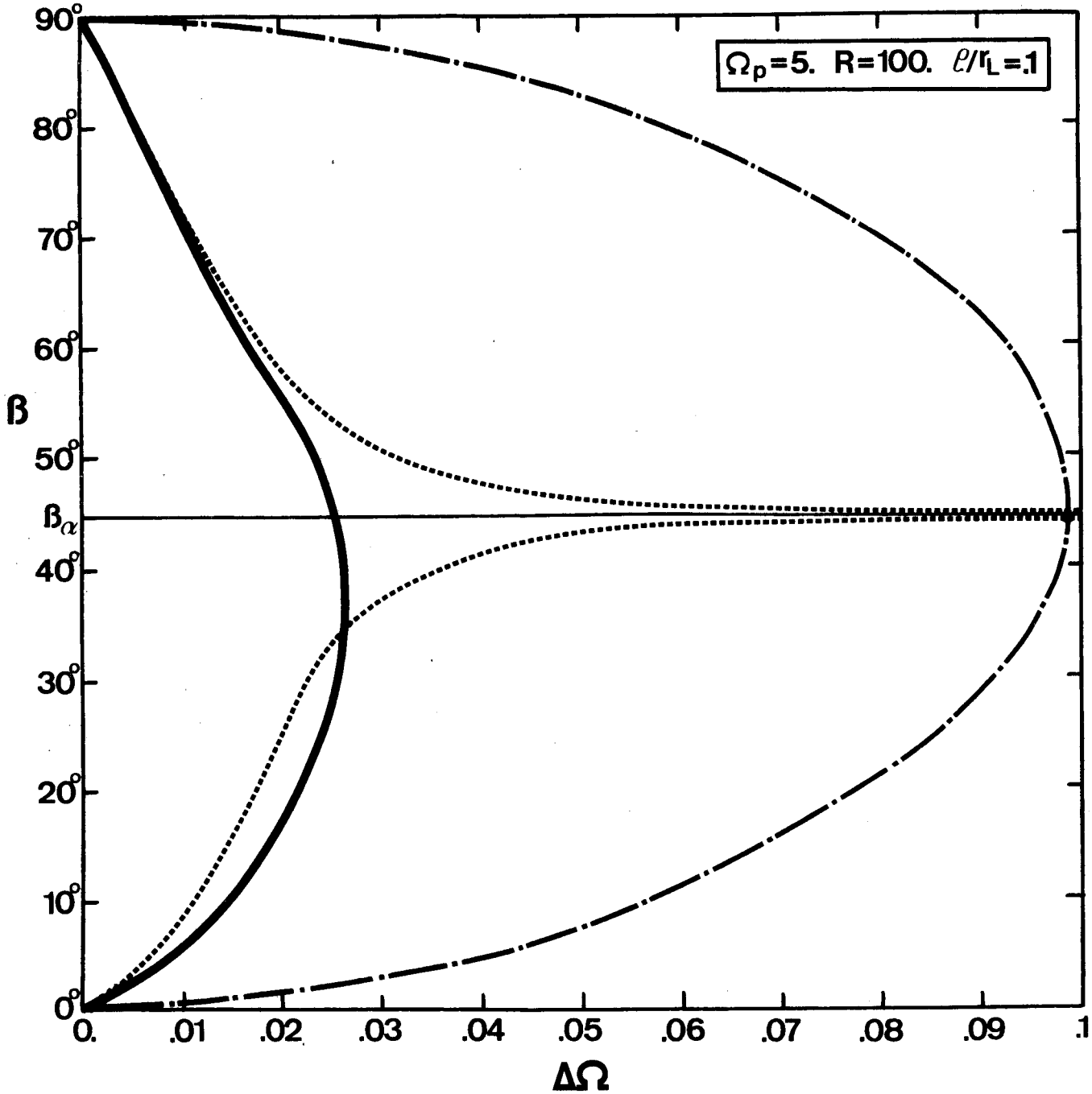
Ω_p=5. R=100. ℓ/r_L=.1
90°
80°
70°
60°
ß
50°
$ß_\alpha$
40°
30°
20°
10°
0°
0.
.01
.02
.03
.04
.05
.06
.07
.08
.09
.1
ΔΩ

Figure 11.

CRPE
Centre de Recherches
en Physique de l'Environnement
terrestre et planétaire

Avenue de la Recherche scientifique
45045 ORLEANS CEDEX

Département PCE
Physique et Chimie
de l'Environnement

Avenue de la Recherche scientifique
45045 ORLEANS CEDEX

Département ETE
Etudes par Télédétection
de l'Environnement

CNET - 38-40 rue du général Leclerc
92131 ISSY-LES-MOULINEAUX

CNET imp 75/1163